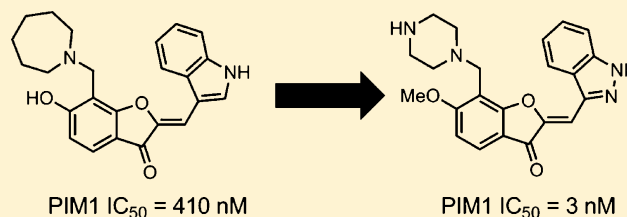


Rational Evolution of a Novel Type of Potent and Selective Proviral Integration Site in Moloney Murine Leukemia Virus Kinase 1 (PIM1) Inhibitor from a Screening-Hit Compound

Hirofumi Nakano,[†] Nae Saito,[†] Lorien Parker,[‡] Yukio Tada,[†] Masanao Abe,[†] Keiko Tsuganezawa,[‡] Shigeyuki Yokoyama,^{‡,§,||} Akiko Tanaka,^{†,‡} Hirotsu Kojima,[†] Takayoshi Okabe,[†] and Tetsuo Nagano^{*,†,⊥}[†]Open Innovation Center for Drug Discovery, The University of Tokyo, 7-3-1 Hongo, Bunkyo-ku, Tokyo 113-0033, Japan[‡]RIKEN Systems and Structural Biology Center, 1-7-22 Suehiro-cho, Tsurumi, Yokohama 230-0045, Japan[§]Laboratory of Structural Biology, and ^{||}Department of Biophysics and Biochemistry, Graduate School of Science, The University of Tokyo, 7-3-1 Hongo, Bunkyo-ku, Tokyo 113-0033, Japan[⊥]Graduate School of Pharmaceutical Sciences, The University of Tokyo, 7-3-1 Hongo, Bunkyo-ku, Tokyo 113-0033, Japan

S Supporting Information

ABSTRACT: Serine/threonine kinase PIM1 is an emerging therapeutic target for hematopoietic and prostate cancer therapy. To develop a novel PIM1 inhibitor, we focused on **1**, a metabolically labile, nonselective kinase inhibitor discovered in our previous screening study. We adopted a rational optimization strategy based mainly on structural information for the PIM1-**1** complex to improve the potency and selectivity. This approach afforded the potent and metabolically stable PIM1-selective inhibitor **14**, which shows only a marginal increase in molecular weight compared with **1** but has a significantly decreased cLogP. The validity of our design concept was confirmed by X-ray structure analysis. In a cellular study, **14** potently inhibited the growth of human leukemia cell line MV4-11 but had a negligible effect on the growth of WI-38 (surrogate for general toxicity). These results demonstrate the effectiveness of our design strategy for evolving the screening-hit compound **1** into a novel type of PIM1 inhibitor, **14**.



■ INTRODUCTION

PIM1, a member of serine/threonine kinase, is an emerging target for cancer therapy.^{1,2} Its expression is increased in patients with hematopoietic and prostate cancer.^{3,4} Enforced expression of PIM1 leads to inhibition of apoptosis and enhancement of cell proliferation,⁵ and PIM1-transgenic mice show increased susceptibility to tumorigenesis.^{6,7} PIM1 has been reported to phosphorylate multiple proteins, such as BAD,⁸ c-MYC,⁹ histone H3,¹⁰ p21^{waf1},¹¹ p27^{kip1},¹² CDC25A,¹³ CDC25C,¹⁴ and CXCR4,¹⁵ resulting in enhanced cell survival, proliferation, and migration. PIM1 also phosphorylates and stabilizes drug efflux transporters, such as P-glycoprotein¹⁶ and BCRP,¹⁷ resulting in drug resistance. Because PIM1-deficient mice do not display any overt abnormalities,¹⁸ these experimental results indicate the potential importance of PIM1 as a therapeutic target for cancer therapy.

There has been increasing interest in PIM1 inhibitors,¹⁹ and typical PIM1 inhibitors reported so far have fused rings as a core such as the imidazo[1,2-*b*]pyridazine ring.^{20,21} Among these inhibitors, SGI-1776 was the most advanced drug candidate²²⁻²⁴ and it is the only PIM1 inhibitor to have been the subject of clinical trials. However, clinical investigation of SGI-1776 was discontinued in 2010 because dose-limiting

toxicity, i.e., cardiac QT prolongation, was identified (<http://clinicaltrials.gov/ct2/show/study/NCT00848601>). Although other chemical classes of PIM1 inhibitor have been reported,²⁵⁻⁴² none is currently under clinical investigation to our knowledge. Therefore, there is still great interest in novel types of small-molecular PIM1 inhibitors.

We identified compound **1** (Figure 1) as a PIM1 inhibitor in a previous screening study (Table 1).⁴³ But, although its potency was acceptable as a starting point for optimization (IC₅₀ = 410 nM), compound **1** showed a poor kinase selectivity profile toward a panel of 50 kinases (see Figure 2 and Table S1, Supporting Information). Because over 500 protein kinases are encoded in the human genome, selectivity is a major concern in the design of kinase inhibitors.⁴⁴ In addition, the metabolic stability of **1** was mediocre in both human and mouse liver microsome systems, with only about 40% recovery after incubation for 1 h. The calculated lipophilicity (cLogP) of **1** is high, 5.3,⁴⁵ and this is considered to be related to the metabolic instability.⁴⁶ Therefore, it is important to minimize any increase in cLogP, or to reduce it if possible, during

Received: January 30, 2012

Published: April 27, 2012



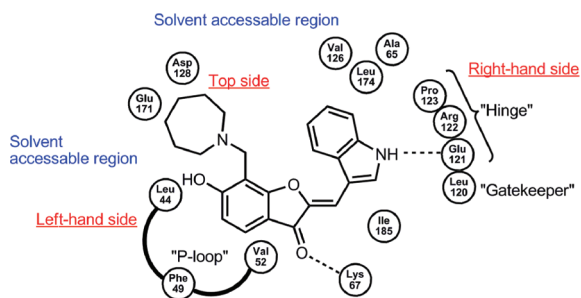


Figure 1. A schematic representation of compound **1** complexed with PIM1 kinase. Dashed lines indicate hydrogen bonds between compound **1** and PIM1.

Table 1. Properties of Compound 1

compd	kinase inhibition		metabolic stability ^a	
	PIM1 IC ₅₀ ^b (nM)	kinase selectivity ^c	HLM ^d (%)	MLM ^e (%)
1	410	low	36	44

^aCarried out at Cerep. Compound was incubated at 37 °C for 1 h with 0.3 mg/mL protein. % remaining was determined by HPLC-MS/MS. ^bIC₅₀ value is shown as the mean of duplicate experiments. [ATP] = 30 μM. ^cFor details, see Figure 2 and Table S1, Supporting Information. ^dHuman liver microsomes. ^eMouse liver microsomes.

optimization of **1**. In general, lower cLogP as well as lower molecular weight (MW) are preferable to achieve good ADMET (absorption, distribution, metabolism, excretion, and toxicity) properties.⁴⁷ However, cLogP and MW generally tend to increase during optimization.⁴⁸

So, as an optimization strategy, we decided to focus first on introducing specific hydrogen-bonding interactions between the compound and the protein in order to improve potency and selectivity and second on reducing the lipophilicity in order to improve the ADMET properties. Further, we aimed to modify the compound in as simple a way as possible in order to minimize the increase of molecular weight. To help us achieve these goals, we planned to utilize structural information, mainly from X-ray analysis of the PIM1-1 complex, to guide the modifications.

Here, we report the rational evolution of **1** into a potent, selective, and metabolically stable PIM1 inhibitor, **14**, using the strategy described above. Compared with the initial screening-hit compound **1**, the new inhibitor **14** showed greatly increased potency and selectivity for PIM1 over other kinases, as well as a significant reduction in cLogP value, with only a marginal increase in molecular weight. In cellular assay, **14** potently

inhibited the growth of human leukemia cell line MV4-11 and induced apoptosis and G1 phase arrest. These results indicate that **14** is a promising lead compound for further study.

RESULTS AND DISCUSSION

Structural Basis of the Inhibitor Design. We solved the crystal structure of PIM1 complexed with **1**, which will be reported separately.⁴⁹ The structure revealed that **1** binds in the ATP-binding cleft. Figure 1 shows a schematic representation of the complex. Briefly, the major interactions with the protein involve the benzofuranone core and the indole ring. Both rings form hydrophobic interactions with the protein: the benzofuranone core with the P-loop and the indole ring through a hydrophobic pocket lined by residues Leu-44, Val-52, Ala-65, Val-126, Leu-174, Ile-185, and C α , C β , C δ , and C γ of Arg-122 and C δ of Pro-123. Both rings also form hydrogen bonds with the protein: the 3-keto group on the benzofuranone core with the side chain of the catalytically essential Lys-67⁵⁰ and the NH in the indole ring with the backbone carbonyl of the hinge residue Glu-121, which usually forms a critical hydrogen bond with the adenine amino group of ATP.⁵¹ These two amino acid residues, Lys-67 and Glu-121 are typically involved in interactions with PIM1 inhibitors.⁵² The phenolic hydroxyl on the left-hand side of the core is located near the edge of the ATP-binding pocket and seems to have no significant interaction with the protein.

The homopiperidine ring on the top side of the core extends into regions following the hinge. These regions have been termed the specificity surface and the ribose-binding region. It has been proposed that targeting the specificity surface can improve the kinase selectivity of inhibitors.^{53–55}

A unique structural feature of PIM kinases is the presence of proline, which cannot donate a hydrogen atom, as the “gatekeeper (gk) +3” residue (Pro-123 in PIM1, Figure 1) at the hinge region.⁵¹ In most cases, kinase inhibitors accept a hydrogen bond from the backbone amide of the gk+3 residue.⁵⁶ It has therefore been proposed that the unusual lack of a hydrogen bond donor at the gk+3 position in PIM can be targeted to design more selective inhibitors.^{36,52}

On the basis of the above structural information, we sought to modify compound **1** to improve its potency and selectivity while retaining key interactions.

Modification of the Top Side of 1. On the basis of the above structural analysis, we initially modified the top side (7-position) of the benzofuranone core (Table 2). As shown in Figure 1, the homopiperidine ring of **1** lies in close proximity to the acidic amino acid residues Asp-128 and Glu-171. Targeting

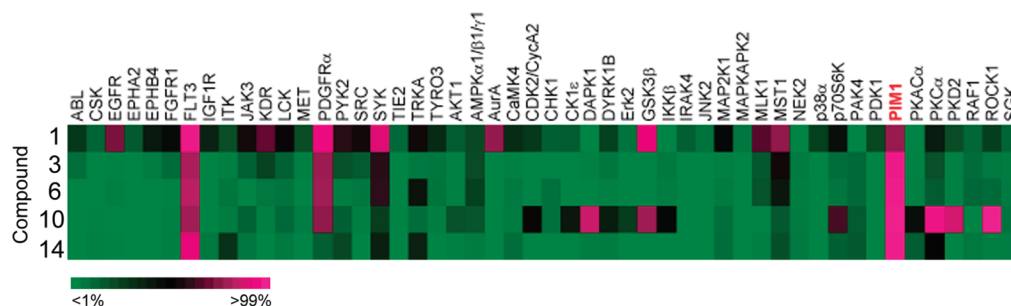
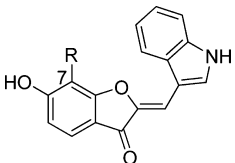
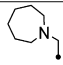
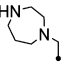
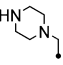
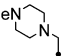


Figure 2. Kinase selectivity profiles of compounds **1**, **3**, **6**, **10**, and **14**. The color-coding scheme is as follows: <1% inhibition (green), 50% inhibition (black), and >99% inhibition (magenta). Selective inhibitor profiles contain fewer magenta elements and more green elements. A complete table with percent inhibition data is available in Supporting Information (Table S1).

Table 2. Structure–Activity Relationship of 7-Substitutes on Benzofuran-3-one core


Compound	R	PIM1 IC ₅₀ (nM) ^a	cLogP ^b	LE ^c	LLE ^d
1		410	5.3	0.31	1.1
2		102	3.4	0.34	3.6
3		17	3.4	0.39	4.4
4		388	4.0	0.31	2.4

^aIC₅₀ values are shown as the mean of duplicate experiments. [ATP] = 30 μM. ^bCalculated logarithm of the octanol/water distribution coefficient using ChemBioDraw Ultra version 11.0.1. ^cLE = $-1.4 \cdot \log_{10}(\text{IC}_{50})/\text{HAC}$; HAC = heavy atom count. ^dLLE = $-\log_{10}(\text{IC}_{50}) - \text{cLogP}$.

Asp-128 is especially attractive in terms of kinase selectivity because Asp-128 is positioned in the specificity surface. We therefore planned to introduce additional hydrogen bonds with Asp-128 and Glu-171 by replacing the homopiperidine ring with a structure having an additional basic amino group. Introduction of an amino group is also expected to reduce the cLogP value of **1**. We first synthesized **2**, which has a 7-membered homopiperazine ring with an amino group at the lateral of the molecule. As expected, **2** showed a 4-fold improvement in potency compared to **1**. Next, we synthesized **3**, which has a 6-membered piperazine ring, and this resulted in a further 6-fold increase in potency (IC₅₀ = 17 nM). We have solved the structure of representative compounds at each step of the ligand-design process and confirmed the lateral NH group on the piperazine ring forms direct hydrogen bonds with the side-chain carboxyl of Asp-128 and the backbone carbonyl of Glu-171 throughout the optimization. In sharp contrast, methylation of the lateral amino group on the piperazine ring, as in compound **4**, dramatically decreased the potency. The piperazine ring in **3** was also found to contribute to the improvement of kinase selectivity (Figure 2). Further, the transition from **1** to **3** reduced the cLogP value from 5.3 to 3.4.

Throughout the optimization process, we monitored the effectiveness of our synthetic effort by calculating ligand efficiency (LE) and ligand lipophilicity efficiency (LLE) values: LE is a measure of the potency with respect to the molecular size, while LLE indicates the balance between potency and lipophilicity.^{57–59} Because we aimed to improve potency while minimizing the increase in MW and reducing cLogP, the easily calculable values of LE and LLE were expected to be useful guides. In the evolution of **1** to **3**, the LE and LLE values were improved from 0.31 to 0.39 and from 1.1 to 4.4, respectively.

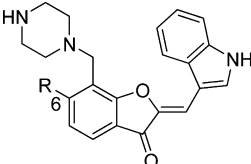
Modification of the Left-Hand Side of the Molecule.

We considered that the left-hand side of **1** might be modified in a variety of ways, as there were no obvious interactions between the compound and the protein. Therefore, we selected the phenolic hydroxyl at the 6-position of the core because it was

expected to be useful as a synthetic handle. From a medicinal chemistry point of view, capping a possibly metabolically labile phenolic hydroxyl group is a favorable modification.

The P-loop is the only region of the protein within potential binding distance from the phenolic hydroxyl group of **1**. In the P-loop, there are only two polar amino acids, Ser-46 and Ser-51. In the crystal structure, the hydroxyl side chains of these residues point away from **1**, toward the aqueous region.⁴⁹ Backbone carbonyls and amides in the P-loop also point toward the aqueous region. Therefore, it would be difficult to introduce additional hydrogen-bonding interactions between the protein and the compound at this site. As an alternative approach, we targeted the P-loop through hydrophobic interactions. The phenolic hydroxyl is located near the edge of the ATP-binding pocket, and so modification with smaller lipophilic substituents seemed preferable. Also, the smaller the lipophilic substituent, the smaller the increase in lipophilicity, which is a key factor for metabolic lability.

As we expected, the size of the lipophilic group was critical for inhibitory potency (Table 3). Removal of the hydroxyl

Table 3. Structure–Activity Relationship of 6-Substitutes on Benzofuran-3-one core


compound	R	PIM1 IC ₅₀ (nM) ^a	cLogP ^b	LE ^c	LLE ^d
3	OH	17	3.4	0.39	4.4
5	H	20	3.8	0.40	3.9
6	OMe	2	3.8	0.42	4.9
7	OEt	6	4.3	0.38	3.9
8	OPr	12	4.9	0.36	3.0
9	OBn	43	5.6	0.29	1.8

^aIC₅₀ values are shown as the mean of duplicate experiments. [ATP] = 30 μM. ^bCalculated logarithm of the octanol/water distribution coefficient using ChemBioDraw Ultra Version 11.0.1. ^cLE = $-1.4 \cdot \log_{10}(\text{IC}_{50})/\text{HAC}$; HAC = heavy atom count. ^dLLE = $-\log_{10}(\text{IC}_{50}) - \text{cLogP}$.

group did not significantly affect the potency, as observed for compound **5**, while methylation increased the potency by 8.5-fold, as in compound **6**. The quality indicators, LE and LLE, were increased to 0.42 and 4.9, respectively. The inhibitory potency decreased as the size of the lipophilic group was increased (compounds **7–9**). Benzyl substitution at this position significantly decreased the potency. A possible explanation is a steric clash between the larger lipophilic groups and the P-loop, which is located 3 Å away from the methyl group at the closest point. Therefore, to be accommodated inside the pocket, bigger groups might have to adopt less energetically favored, possibly twisted conformations.

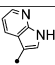
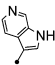
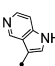
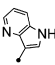
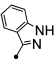
Compound **6**, which has the 6-methoxy group on the left-hand side of the core, was selected for further modifications based on the improvement of potency, LE, and LLE, compared with **1**.

Modification of the Right-Hand Side of the Molecule.

The right-hand side of **1** offers fewer options for modification because the parent indole ring forms the critical hydrogen bond

with Glu121 and has various hydrophobic interactions with the protein. Therefore, we sought to modify the right-hand side without disrupting these critical interactions. Researchers at Plexikon have reported the crystal structure of the PIM1 complex with a 7-azaindole compound. Their compound binds to the ATP-binding site of PIM1 in the same orientation as **1**, forming a hydrogen bond between the NH group and Glu-121 (PDB ID: 3C4E).⁶⁰ Thus, we replaced the indole ring of **6** with a 7-azaindole ring. The resulting 7-azaindole derivative, **10**, inhibited PIM1 as potently as **6** (Table 4). In general,

Table 4. Kinase Inhibitory Activity of Azaindole Derivatives

Compound	R	PIM1 IC ₅₀ (nM) ^a	cLogP ^b	LE ^c	LLE ^d
10		2	2.8	0.42	5.9
11		92	2.8	0.34	4.2
12		53	2.8	0.35	4.5
13		447	3.1	0.31	3.2
14		3	3.3	0.41	5.2

^aIC₅₀ values are shown as the mean of duplicate experiments. [ATP] = 30 μM. ^bCalculated logarithm of the octanol/water distribution coefficient using ChemBioDraw Ultra version 11.0.1. ^cLE = -1.4·log₁₀(IC₅₀)/HAC; HAC = heavy atom count. ^dLLE = -log₁₀(IC₅₀) - cLogP.

replacement of a carbon atom with a nitrogen atom, while maintaining the molecular size, reduces the lipophilicity. However, as can be deduced from Figure 1, introduction of a nitrogen atom that faces the hinge region, as in **10**, may cause a kinase selectivity problem because the nitrogen atom can act as a hydrogen bond acceptor for kinases with a hydrogen bond donor at this site.

With this selectivity concern in mind, we next explored other azaindole derivatives. The 6-, 5-, and 4-azaindole derivatives, **11**, **12**, and **13**, showed decreased potency (Table 4), while the indazole (2-azaindole) derivative, **14**, inhibited PIM1 as potently as **6** or **10**.

The cLogP values for **10** and **14** are 2.8 and 3.3, respectively, both of which are lower than that of **6**. The reduction in cLogP values of **10** and **14** was associated with an improvement of the LLE values to 5.9 and 5.2, respectively, from the value of 4.9 in **6**, and the LE values were maintained.

Kinase Selectivity Study. Kinase selectivity data are summarized in Figure 2 and Table S1, Supporting Information. Each compound was tested against a panel of 20 tyrosine kinases and 30 serine/threonine kinases at a concentration 50-fold higher than the IC₅₀ value in the PIM1 inhibitory assay (carried out at CarnaBiosciences, Japan). The ATP concentration used was approximately equal to the K_m value for each kinase. As mentioned earlier, **1** showed a poor kinase selectivity profile, inhibiting tyrosine kinases FLT3, PDGFRα, SYK, and

the serine/threonine kinase GSK3β more potently than PIM1. In addition, **1** inhibited other tyrosine kinases, EGFR, KDR, and serine/threonine kinases Aurora A, MLK1, and MST1, as potently as PIM1.

Introduction of a piperazine ring on the top side of the core resulted in a marked improvement in selectivity. The selectivity profile of **3** showed that it inhibited PIM1 most potently among the kinases examined. However, FLT3, PDGFRα, and SYK were still potently inhibited by **3**. Modification of the left-hand side of the core, specifically methylation of the hydroxyl at the 6-position, did not significantly change the selectivity (**3** vs **6**).

The two azaindole derivatives, **10** and **14**, showed a significant difference in the kinase selectivity profile. As expected, the 7-azaindole derivative **10** showed a nonspecific selectivity profile compared to **3** and **6**, presumably owing to hydrogen bond formation with the backbone amide of the gk+3 residue in off-target kinases. In addition to FLT3 and PDGFRα, **10** potently inhibited serine/threonine kinases DAPK1, GSK3β, PKCα, PKD2, and ROCK1. In contrast, **14**, the indazole (2-azaindole) derivative showed a much cleaner selectivity profile. Other than PIM1, only FLT3 was potently inhibited by **14**. Under the assay conditions used, **14** inhibited PIM1 and FLT3 with IC₅₀ values of 6 nM and 47 nM, respectively. The clinically tested PIM1 inhibitor SGI-1776 shows similar potency and selectivity characteristics with respect to FLT3.^{22–24}

All our compounds tested showed selectivity for PIM1 and PIM3 over PIM2 (Table 5). In the case of **14**, the IC₅₀ values

Table 5. Pim Family Selectivity Study^a

kinase	ATP concn (μM) ^b	rate of inhibition (%) ^c				
		1	3	6	10	14
PIM1	500	77	98	99	>99	99
PIM2	5	46	30	30	39	19
PIM3	150	88	97	98	99	98

^aCarried out at CarnaBiosciences. ^bATP concentration was approximate K_m value of each kinase. ^cThe rate of enzyme inhibition was examined by an electrophoretic mobility shift assay. Each compound was tested at the concentration which is 50 times higher than its PIM1 IC₅₀ value. The concentration of each compound was; **1**, 22500 nM; **3**, 600 nM; **6**, 250 nM; **10**, 200 nM; **14**, 300 nM. PIM1 IC₅₀ values for this study were determined at CarnaBiosciences.

for PIM2 and PIM3 were 1160 and 13 nM, respectively. Again, the same tendency has been reported for SGI-1776.^{22–24} At the amino acid level, PIM2 is 53% identical to PIM1 and PIM3 is 71% identical to PIM1.^{1,19} PIM2 is mainly expressed in hematological and prostate cancer cells as PIM1, and PIM3 is highly expressed in hepatic and pancreatic cancer cells.¹ The concept of the inhibition of all three PIM family members has been proposed in consideration of the functional redundancy and potential compensatory mechanism of PIM family members.³⁶ However, the functional redundancy of PIM family members in cancer biology remains unclear.¹ For example, PIM1 deficient mice show a lower level of CXCR4 expression on the surface of the bone marrow cells, which is not compensated by the presence of PIM2.¹⁵

Finally, compound **14**, which showed potent PIM1-inhibitory activity and a clean kinase selectivity profile, was selected as the most promising lead candidate.

Cellular Study. To evaluate the cellular activity of **14**, we carried out growth inhibition assay using the human leukemia

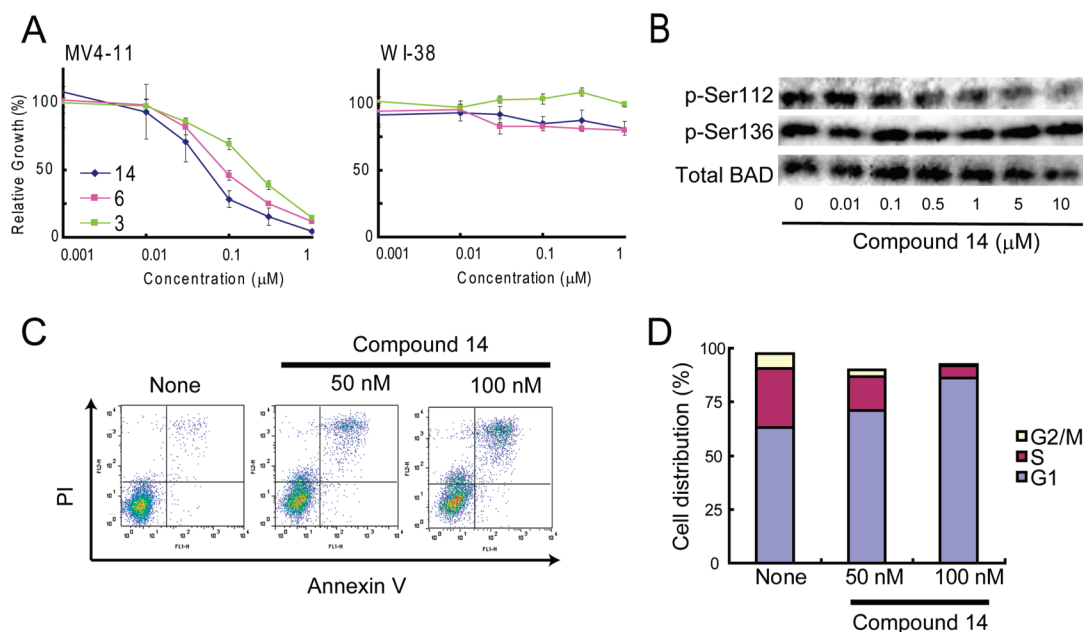


Figure 3. Cellular study of compound 14. (A) Growth inhibition assay with MV4–11 cells. Cells were counted with a Cell Counting Kit-8. WI-38 cells were used as a control. (B) Inhibition of phosphorylation of BAD at Ser-112. MV4–11 cells were treated with various concentrations of 14 for 1 h, and protein extracts were subjected to immunoblotting. (C) MV4–11 cells were treated with 14 for 48 h. Induction of apoptosis was evaluated with Annexin V and PI staining. (D) Cell cycle distribution of MV4–11 cells after 48 h treatment with 14.

Table 6. ADMET Profiling Data for Compound 14^a

metabolic stability ^b (%)			CYP inhibition ^c (%)					hERG inhibition ^d (%)	
liver microsomes ^e		hepatocytes ^f	1A2	2C9	2C19	2D6	3A4	10 μM	1 μM
human	mouse	mouse							
>99	92	89	33	<1	54	11	10	60	13

^aADMET study was carried out at Cerep. ^bCompound concentration was 1 μM. %Remainings of the compound was determined by HPLC-MS/MS. ^cCompound concentration was 10 μM. ^dA patch-clamp method was carried out to evaluate hERG inhibition. ^eCompound was incubated with 0.3 mg/mL protein at 37 °C for 1 h. ^fCryopreserved hepatocytes. Compound was incubated with 1 million cells/mL at 37 °C for 2 h.

cell line MV4–11, which is frequently used to evaluate the efficiency of PIM1 inhibitors (Figure 3A). Compound 14 potentially inhibited the growth of MV4–11 (GI₅₀ = 43 nM) and had only a negligible effect on the growth of the normal human diploid lung fibroblast cell line WI-38, which was used as a surrogate for general toxicity. In comparison, 6, which inhibited PIM1 as potently as 14, showed a reduced ability to inhibit the growth of MV4–11 (GI₅₀ = 95 nM). Compound 3 showed weak inhibition of MV4–11 cell growth (GI₅₀ = 270 nM), which was not unexpected as it is a weaker PIM1 inhibitor. On the basis of these results, 14 was prioritized for further study.

Next, we examined the phosphorylation status of BAD to confirm the inhibition of PIM1 in MV4–11 cells. PIM1 is reported to phosphorylate BAD at Ser-112, thereby deactivating the pro-apoptotic function of BAD.⁶¹ Compound 14 was incubated with MV4–11 for 1 h, and cells were lysed for analysis of their phosphorylation status by Western blotting. As shown in Figure 3B, 14 dose-dependently inhibited the phosphorylation of BAD at Ser-112 but not at Ser-136. It was also confirmed to induce apoptosis (Figure 3C) and cell-cycle arrest at the G1 phase (Figure 3D) in a dose-dependent manner, as has been found for other PIM1 inhibitors.^{22–24,29}

ADMET Study. Compound 14 showed an acceptable ADMET profile (Table 6). First, its metabolic stability in liver microsomes was greatly improved compared with that of 1, as expected from the reduction in cLogP by 2 log units. It

was very stable and was almost quantitatively recovered after incubation with both human (>99%) and mouse liver microsomes (92%), whereas recovery of 1 was only about 40% in both cases (Table 1). Other potent and selective PIM1 inhibitors, compound 3 and 6, were less stable compared to 14. Compound 3 was recovered in 90% in human liver microsomes and 71% in mouse liver microsomes. Compound 6 was recovered in 82% in human liver microsomes and 86% in mouse liver microsomes. In addition, 14 was stable in the presence of cryopreserved hepatocytes, which mimic in vivo metabolic conditions due to their retention of a complete ensemble of metabolizing enzymes and other cellular components.⁶² Second, 14 did not potently inhibit five major cytochrome P450 (CYP) enzymes at 10 μM, indicating that it has low potential for drug–drug interactions. Third, 14 showed only moderate inhibition of potassium channel hERG (human ether-a-go-go related gene). hERG is a cardiac potassium ion channel, and its inhibition may trigger life-threatening torsades de pointes (TdP) arrhythmia through QT prolongation.⁶² Compound 14 inhibited hERG to the extent of 60% at 10 μM and only 13% at 1 μM, whereas SGI-1776, whose clinical investigations were discontinued due to QT prolongation, is reported to inhibit hERG more potently than this (IC₅₀ = 0.98 μM).⁶³

Structural Study. Compound 14 (PDB ID: 3UMW) binds in the ATP-binding cleft at the same site as compound 1

(Figure 4), and it retains the representative hydrophobic interactions and hydrogen bonds seen in the complex of **1** and

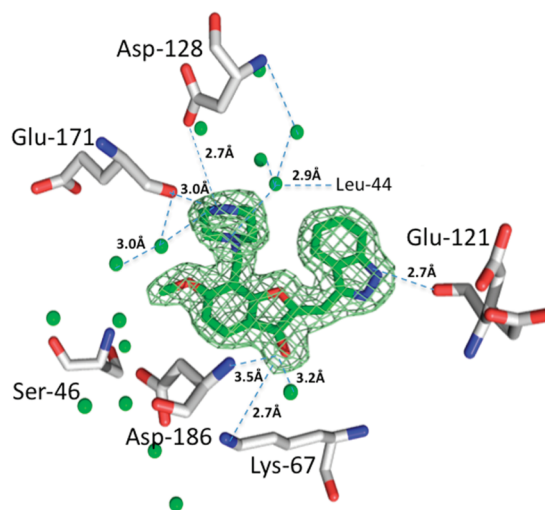


Figure 4. Electron density and hydrogen-bonding interactions between compound **14** and PIM1 kinase. Compound **14** is represented by green sticks, while the protein residues are colored gray. Nitrogen and oxygen are colored blue and red, respectively. Water molecules are displayed as green spheres. Interactions are drawn as dashed lines, and distances are given in Å. Electron density is represented as a green mesh and was calculated using an omit map contoured to $1-\sigma$.

PIM1. Importantly, the distance between the ring and Glu-121 is shorter in **14** than in **1**.⁴⁹

On the top side, the piperazine ring, which is a critical substituent for potency and selectivity, forms two hydrogen bonds with the protein, as anticipated. The nitrogen atom at the top of the ring forms hydrogen bonds with the side-chain carboxyl of Asp-128 and the backbone carbonyl of Glu-171. The decreased potency of **4**, in which the lateral nitrogen atom in the piperazine ring is methylated, supports the importance of both hydrogen bonds. Replacement of the 6-membered piperazine with 7-membered homopiperazine resulted in a 6-fold reduction of potency, as seen with **2** (Table 2). In the structure of the compound **1** complex, the 7-membered ring

showed less well-defined electron density, presumably due to increased flexibility of the 7-membered ring compared to that of the 6-membered ring.⁴⁹ It seems likely that the homopiperazine ring would behave similarly and may also bind with both Asp-128 and Glu-171, but there would be a higher entropy penalty as compared to the piperazine ring in compound **14**. Although the contribution to selectivity was not mentioned, Qian and co-workers reported that the side-chain carboxyl of Asp-128 and backbone carbonyl of Glu-171 exhibit a water-mediated interaction with their PIM1 inhibitors.³¹ In addition, during the preparation of this manuscript, Xiang and co-workers reported that hydrogen bonds with those two amino acid residues are key interactions of their potent PIM1 inhibitors.³⁵

On the left-hand side of the molecule, the methyl group at the 6-position of the core is accommodated inside the hydrophobic pocket and participates in interactions between the core and the P-loop, which improves the potency, as seen in the comparison of **3** and **6** (Table 3).

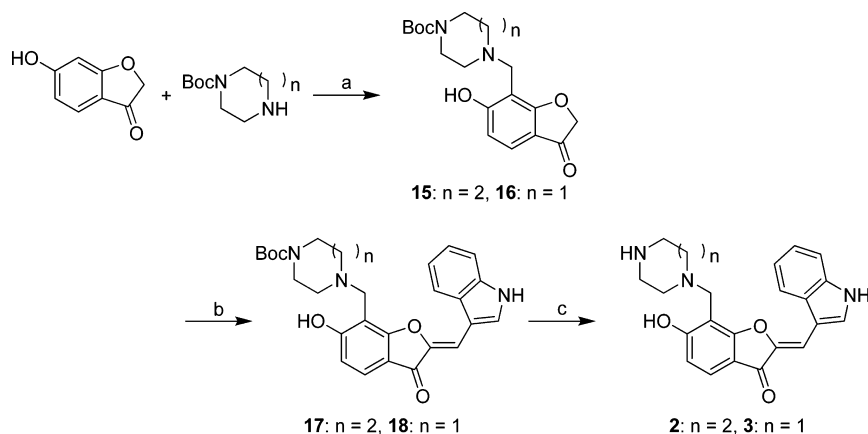
Judging from currently available information, no other reported compound makes as many simultaneous interactions with PIM1 as **14**, namely direct H-bonds with Lys-67, Glu-121, Asp-128, and Glu-171.

Chemistry. Compounds **2** and **3** were synthesized as shown in Scheme 1. Mannich reaction of 6-hydroxy-2*H*-benzofuran-3-one with paraformaldehyde and *N*-Boc-homopiperazine or *N*-Boc-piperazine provided intermediates **15** and **16**. Knoevenagel condensation with 1*H*-indole-3-carbaldehyde afforded **17** and **18**. Subsequent acidic removal of a Boc group furnished **2** and **3**.

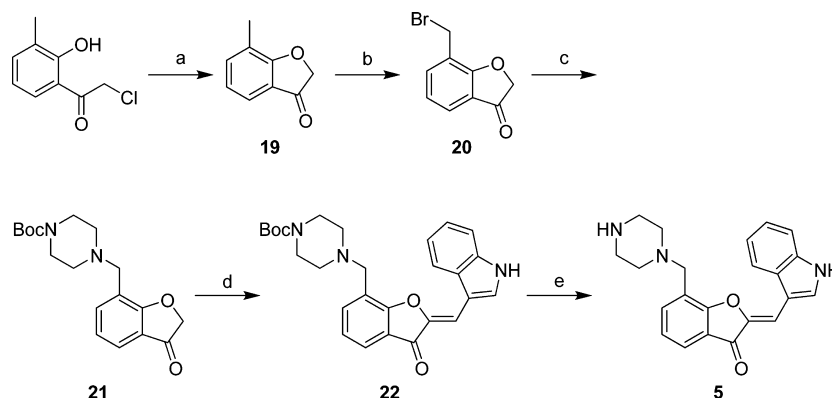
An analogue unsubstituted at the 6-position of the benzofuranone core, **5**, was synthesized according to Scheme 2. Basic cyclization of 2-chloro-1-(2-hydroxy-3-methylphenyl)ethanone⁶⁴ afforded **19**. Bromination at the benzyl position of **19** was carried out with *N*-bromosuccinimide (NBS) and benzoyl peroxide (BPO) in refluxing CCl_4 to afford **20**. Replacement of bromide with *N*-Boc-piperazine furnished **21**, which was condensed with 1*H*-indole-3-carbaldehyde to afford **22**. Finally, acidic removal of the Boc group of **22** furnished **5**.

6-Alkoxyated benzofuranone derivatives were synthesized according to Scheme 3. The 6-hydroxyl group of **16** was alkylated by Mitsunobu reaction with various alcohols.

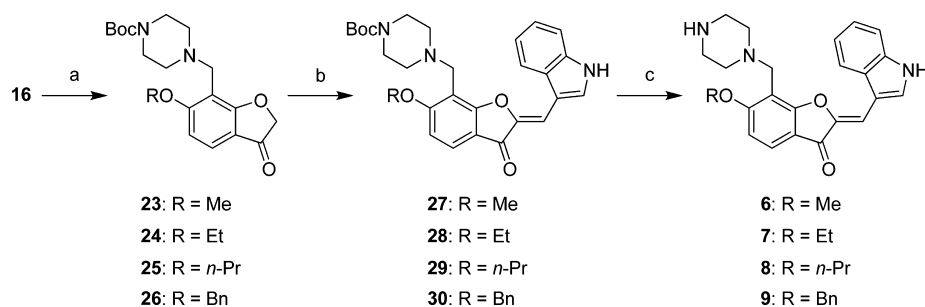
Scheme 1. Synthesis of 7-Modified Derivatives **2** and **3**^a



^aReagents and conditions: (a) paraformaldehyde, EtOH, 120 °C under microwave irradiation, 15% (**15**) or reflux, 52% (**16**); (b) 1*H*-indole-3-carbaldehyde, piperidine, MeOH, 60 °C, 28% (**17**) and 68% (**18**); (c) 4*N* HCl in dioxane, CH_2Cl_2 , rt, 50% (**2**) and 75% (**3**).

Scheme 2. Synthesis of 6-Unsubstituted Derivative 5^a

^aReagents and conditions: (a) K_2CO_3 , CH_3CN , rt, 43%; (b) NBS, BPO, CCl_4 , reflux, 36%; (c) *N*-Boc-piperazine, CH_2Cl_2 , rt, quant; (d) 1*H*-indole-3-carbaldehyde, piperidine, MeOH, 60 °C, 76%; (e) 4*N* HCl in dioxane, CH_2Cl_2 , rt, 67%.

Scheme 3. Synthesis of 6-Alkoxy Derivatives 6–9^a

^aReagents and conditions: (a) ROH, PPh_3 , DEAD, toluene, 110 °C, 28–43%; (b) 1*H*-indole-3-carbaldehyde, piperidine, MeOH, 60 °C, 53–77%; (c) 4*N* HCl in dioxane, CH_2Cl_2 , rt, 53–80%.

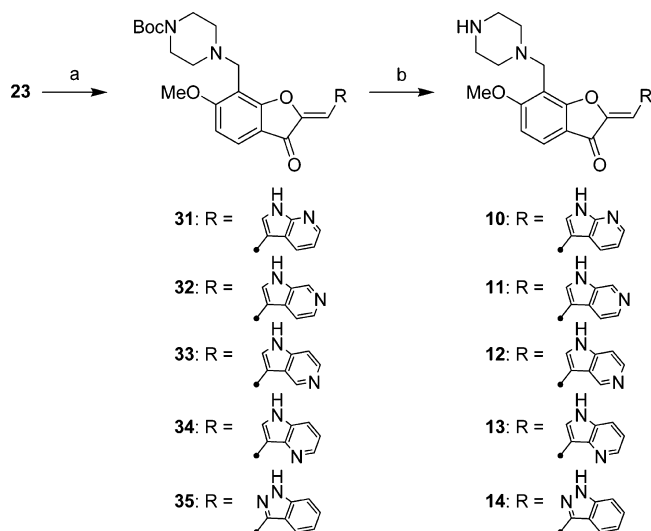
Subsequent Knoevenagel condensation and acidic deprotection afforded compounds 6–9.

Azaindole analogues 10–14 were synthesized as shown in Scheme 4. 23 was condensed with various azaindole-3-carbaldehydes. Subsequent removal of the Boc group afforded 10–14. Among azaindole-3-carbaldehydes, 7-azaindole-3-car-

baldehyde and indazole-3-carbaldehyde were purchased. 4-Azaindole-3-carbaldehyde and 5-azaindole-3-aldehyde were synthesized according to the literature.⁶⁵ 6-Azaindole-3-carbaldehyde was synthesized by formylation of a parent 6-azaindole similarly to 4-azaindole-3-carbaldehyde.

CONCLUSIONS

We evolved 1 into 14, which is about 100 times more potent and much more selective for PIM1, by means of simple chemical modifications guided by structural information. We employed a rational optimization strategy, aiming to introduce specific hydrogen-bonding interactions between the compound and the protein to improve potency and selectivity and to modify the compound in as simple a way as possible in order to minimize the increase of molecular weight as well as to reduce lipophilicity. The validity of our design concept was confirmed by X-ray crystallography, which showed that the incorporated groups participate in interactions with the protein as expected. The molecular weight was increased by only 2 Da, while cLogP was greatly reduced by 2 log units. The reduction of cLogP is mirrored by a significant improvement in metabolic stability. The effectiveness of our modifications was also reflected in the quality indicators LE and LLE: the LE value was increased from 0.31 to 0.41 and LLE from 1.1 to 5.2. In addition, 14 was active in cellular assay, potently inhibiting the growth of the leukemia cell line MV4–11. Further cell-based analysis using MV4–11 confirmed that 14 inhibited the phosphorylation of the typical PIM1 substrate BAD and induced apoptosis and cell cycle arrest at the G1 phase.

Scheme 4. Synthesis of Azaindole Derivatives 10–14^a

^aReagents and conditions: (a) RCHO, piperidine, MeOH, 60 °C, 33–82%; (b) 4*N* HCl in dioxane, CH_2Cl_2 , rt, 12–78%.

Our results provide an example of successful rational compound evolution through simple, structure-guided chemical modifications. By introducing hydrogen-bonding and hydrophobic modifications at appropriate sites, while minimizing the increase of molecular size and decreasing the lipophilicity, we achieved significant improvements in potency, selectivity, and metabolic stability.

EXPERIMENTAL SECTION

General Information. Reagents and solvents were purchased from commercial sources and used without further purification. All reactions were performed under an argon atmosphere unless otherwise noted. Microwave irradiation was carried out with an Initiator (Biotage). Reactions were monitored by thin layer chromatography (TLC) on precoated TLC glass plates (silica gel 60 F254, 250 μ m thickness). Column chromatography was carried out with Yamazen YFLC wprep 2XY on silica gel unless otherwise noted. ^1H NMR spectra were recorded on either a JEOL JNM-LA300 or a JEOL JNM-LA400; chemical shifts (δ) are reported relative to a signal of Me_4Si . Data for NMR are reported as follows: chemical shift (δ ppm), multiplicity (s = singlet, br s = broad singlet, d = doublet, t = triplet, q = quartet, dd = doublet of doublets, m = multiplet or overlapping), coupling constant (Hz), integration. Mass spectra (ESI $^+$) were measured with a JEOL JMS-T100LC mass spectrometer. The purity of compounds was determined by HPLC analysis. The HPLC instrument was composed of a Leap HTS PAL 96-well plate injector (CTC Analysis), HPLC pump model P580 (Dionex), HPLC column thermostat STH 585 (Dionex), HPLC photodiode array detector (Dionex), and Chromleon HPLC data system (Dionex), and was equipped with a Keystone Scientific Prism RPN 4 mm \times 20 mm guard column. The column temperature was 21 $^\circ\text{C}$. The purity measurements were done by measuring peak area at 230 nm, and purity was calculated based on the observed target peak area as a percentage of total area. Mobile phase A consisted of 12.0 mM ammonium formate/5.9 mM formic acid in water. Mobile phase B consisted of 6.7 mM ammonium formate/3.3 mM formic acid in water/ CH_3CN (5/40, v/v). Gradient conditions were as follows: 0% mobile phase B at time of injection; linear increase to 82.5% B at 1.20 min; linear increase to 90% B at 1.60 min; maintain 90% B until 1.80 min. The flow rate was 2.5 mL/min. For compound 12, ACQUITY UPLC (Waters) equipped with an ACQUITY UPLC BEH C18 column was used to determine the purity. The column temperature was 40 $^\circ\text{C}$. Mobile phase A consisted of 5.0 mM ammonium acetate in water. Mobile phase B consisted of CH_3CN . Gradient conditions were as follows: 5% mobile phase B at time of injection; linear increase to 95% B at 1.00 min; maintain 95% B until 1.50 min. The flow rate was 0.7 mL/min. The purity measurements were done by measuring peak area at 230 nm, and purity was calculated based on the observed target peak area as a percentage of total area. All compounds assayed were $\geq 95\%$ pure.

Compound 1 was purchased from InterBioScreen Ltd. (catalogue ID: STOCK6S-34005). Compound 4 was purchased from Princeton Biomolecular Research, Inc. (catalogue ID: OSSK_865988). 7-azaindole-3-carbaldehyde and indazole-3-carbaldehyde were purchased from Aldrich and Apollo Scientific, respectively.

(Z)-2-[(1H-Indol-3-yl)methylene]-7-(azepan-1-ylmethyl)-6-hydroxybenzofuran-3(2H)-one (1). ^1H NMR (300 MHz, $\text{DMSO}-d_6$) δ 1.62 (m, 4H), 1.72 (m, 4H), 2.93 (t, J = 5.1 Hz, 4H), 4.21 (s, 2H), 6.52 (d, J = 8.7 Hz, 1H), 7.11 (s, 1H), 7.15–7.25 (m, 2H), 7.45–7.51 (m, 2H), 8.02 (d, J = 8.1 Hz, 1H), 8.12 (d, J = 2.4 Hz, 1H), 11.89 (br s, 1H).

HRMS (ESI $^+$) calcd for ($\text{C}_{23}\text{H}_{24}\text{N}_3\text{O}_3$) [$\text{M} + \text{H}$] $^+$ 389.1865; found 389.1817.

(Z)-2-[(1H-Indol-3-yl)methylene]-6-hydroxy-7-[(4-methylpiperazin-1-yl)methyl]benzofuran-3(2H)-one (4). ^1H NMR (300 MHz, $\text{DMSO}-d_6$) δ 2.17 (s, 3H), 2.31–2.43 (m, 4H), 2.59–2.69 (m, 4H), 3.94 (s, 2H), 6.67 (d, J = 8.7 Hz, 1H), 7.15–7.26 (m, 3H), 7.49–7.53 (m, 2H), 8.08 (d, J = 8.1 Hz, 1H), 8.16 (d, J = 2.1 Hz, 1H), 11.96 (br s, 1H).

HRMS (ESI $^+$) calcd for ($\text{C}_{23}\text{H}_{24}\text{N}_3\text{O}_3$) [$\text{M} + \text{H}$] $^+$ 390.1818; found 390.1771.

Compounds 2, 3, 5–14 were synthesized as follows.

tert-Butyl 4-[(6-Hydroxy-3-oxo-2,3-dihydrobenzofuran-7-yl)methyl]-1,4-diazepane-1-carboxylate (15). A mixture of 6-hydroxy-2H-benzofuran-3-one (1.50 g, 10.0 mmol), paraformaldehyde (0.300 g, 10.0 mmol), and *N*-Boc-homopiperazine (2.00 g, 10.0 mmol) in EtOH (10 mL) was heated at 120 $^\circ\text{C}$ under microwave irradiation for 20 min. The mixture was concentrated in vacuo, and the resulting residue was purified by column chromatography (0–100% EtOAc/hexane) to afford the title compound (549 mg, 15%).

^1H NMR (300 MHz, CD_3OD) δ 1.47 (s, 9H), 1.78–1.85 (m, 2H), 2.91–2.94 (m, 2H), 2.96–2.99 (m, 2H), 3.47–3.52 (m, 2H), 3.58 (t, J = 5.1 Hz, 2H), 4.65 (s, 2H), 4.92 (s, 2H), 6.49 (d, J = 8.8 Hz, 1H), 7.42 (d, J = 8.8 Hz, 1H).

tert-Butyl 4-[(6-Hydroxy-3-oxo-2,3-dihydrobenzofuran-7-yl)methyl]piperazine-1-carboxylate (16). A mixture of 6-hydroxy-2H-benzofuran-3-one (10.0 g, 66.6 mmol), paraformaldehyde (2.00 g, 66.6 mmol), and *N*-Boc-piperazine (12.4 g, 66.6 mmol) in EtOH (70 mL) was refluxed for 4 h. The mixture was concentrated in vacuo, and the resulting residue was purified by column chromatography (0–50% EtOAc/hexane) to afford 15.6 g of a crude product. The crude product was recrystallized from EtOAc to furnish the title compound (12.1 g, 52%).

^1H NMR (300 MHz, $\text{DMSO}-d_6$) δ 1.38 (s, 9H), 2.44 (m, 4H), 3.32 (m, 4H), 3.66 (s, 2H), 4.73 (s, 2H), 6.59 (d, J = 8.8 Hz, 1H), 7.40 (d, J = 8.8 Hz, 1H).

(Z)-tert-Butyl 4-[(2-[(1H-Indol-3-yl)methylene]-6-hydroxy-3-oxo-2,3-dihydrobenzofuran-7-yl)methyl]-1,4-diazepane-1-carboxylate (17). A mixture of 15 (155 mg, 0.428 mmol), 1H-indole-3-carbaldehyde (62.1 mg, 0.428 mmol), and piperidine (3.64 mg, 0.0428 mmol) in MeOH (2 mL) was heated at 60 $^\circ\text{C}$ for 2 h. The mixture was cooled to room temperature and concentrated in vacuo, and the resulting residue was purified by column chromatography (0%–2% MeOH/ CHCl_3) to afford the title compound (59.1 mg, 28%).

^1H NMR (400 MHz, CDCl_3) δ 1.48 (s, 9H), 1.95 (m, 2H), 2.82–2.89 (m, 4H), 3.51–3.63 (m, 4H), 4.08 (d, J = 17.6 Hz, 2H), 6.66 (d, J = 8.8 Hz, 1H), 7.23–7.30 (m, 3H), 7.45 (d, J = 7.8 Hz, 1H), 7.63 (d, J = 8.3 Hz, 1H), 7.89 (d, J = 7.8 Hz, 1H), 7.98 (d, J = 10.8 Hz, 1H), 9.11 (br s, 1H).

(Z)-tert-Butyl 4-[(2-[(1H-Indol-3-yl)methylene]-6-hydroxy-3-oxo-2,3-dihydrobenzofuran-7-yl)methyl]piperazine-1-carboxylate (18). A mixture of 16 (348 mg, 1.00 mmol), 1H-indole-3-carbaldehyde (145 mg, 1.00 mmol), and piperidine (68.1 mg, 0.0800 mmol) in MeOH (4 mL) was heated at 60 $^\circ\text{C}$ for 2 h. The mixture was cooled to room temperature, and the precipitate was collected by filtration to afford the title compound (324 mg, 68%).

^1H NMR (300 MHz, $\text{DMSO}-d_6$) δ 1.38 (s, 9H), 2.53 (m, 4H), 3.35 (m, 4H), 3.87 (s, 2H), 6.72 (d, J = 8.8 Hz, 1H), 7.14–7.25 (m, 3H), 7.50 (d, J = 8.8 Hz, 1H), 7.53 (d, J = 8.1 Hz, 1H), 8.09 (d, J = 8.1 Hz, 1H), 8.16 (d, J = 2.9 Hz, 1H), 11.98 (br s, 1H).

(Z)-7-[(1,4-Diazepan-1-yl)methyl]-2-[(1H-indol-3-yl)methylene]-6-hydroxybenzofuran-3(2H)-one (2). To 17 (56.0 mg, 0.114 mmol) in CH_2Cl_2 (6 mL) was added 4 N HCl in dioxane (6 mL) at room temperature. The mixture was stirred at the same temperature for 2 h and concentrated in vacuo. Then, 4 mL of triethylamine and 6 mL of toluene were added to the flask, and the resulting mixture was concentrated in vacuo. This process was repeated twice. The residue was purified by column chromatography (0–10% MeOH/ CHCl_3) on NH_2 -modified silica gel to afford the title compound (22.2 mg, 50%).

^1H NMR (400 MHz, $\text{DMSO}-d_6$) δ 1.78 (m, 2H), 2.88–2.94 (m, 8H), 4.11 (s, 2H), 6.46 (d, J = 8.3 Hz, 1H), 7.04 (s, 1H), 7.15–7.24 (m, 2H), 7.41 (d, J = 8.8 Hz, 1H), 7.49 (d, J = 7.8 Hz, 1H), 8.03 (d, J = 7.3 Hz, 1H), 8.10 (s, 1H).

HRMS (ESI $^+$) calcd for ($\text{C}_{23}\text{H}_{24}\text{N}_3\text{O}_3$) [$\text{M} + \text{H}$] $^+$ 390.1818; found 390.1791.

(Z)-2-[(1H-Indol-3-yl)methylene]-6-hydroxy-7-(piperazin-1-ylmethyl)benzofuran-3(2H)-one (3). To a suspension of 18 (143 mg, 0.300 mmol) in CH_2Cl_2 (14 mL) was added 4 N HCl in dioxane (14 mL) at room temperature. The mixture was stirred at the same

temperature for 2 h and concentrated in vacuo. Then 14 mL of saturated aqueous NaHCO₃ was added. The precipitated yellow powder was collected by filtration, washed with water, and dried in vacuo to afford the title compound as a yellow powder (85.2 mg, 75%).

¹H NMR (300 MHz, DMSO-*d*₆) δ 2.59 (m, 4H), 2.80 (m, 4H), 3.92 (s, 2H), 6.59 (d, *J* = 8.1 Hz, 1H), 7.12 (s, 1H), 7.14–7.26 (m, 2H), 7.46–7.51 (m, 2H), 8.07 (d, *J* = 8.1 Hz, 1H), 8.14 (s, 1H), 11.95 (br s, 1H).

HRMS (ESI⁺) calcd for (C₂₂H₂₂N₃O₃) [M + H]⁺ 376.1661; found 376.1645.

7-Methylbenzofuran-3(2H)-one (19). A mixture of 2-chloro-1-(2-hydroxy-3-methylphenyl)ethanone (6.40 g, 34.7 mmol) and K₂CO₃ (14.4 g, 104 mmol) in CH₃CN (170 mL) was stirred at room temperature for 1 h, then filtered. The filtrate was concentrated in vacuo, and the resulting residue was purified by column chromatography (0–10% EtOAc/hexane) to afford the title compound (2.23 g, 43%).

¹H NMR (300 MHz, CDCl₃) δ 2.33 (s, 3H), 4.64 (s, 2H), 7.00 (m, 1H), 7.42 (d, *J* = 7.3 Hz, 1H), 7.51 (d, *J* = 8.0 Hz, 1H).

7-(Bromomethyl)benzofuran-3(2H)-one (20). A mixture of benzoyl peroxide (BPO) (8.90 mg, 0.0500 mmol) and *N*-bromosuccinimide (NBS) (291 mg, 1.20 mmol) in CCl₄ (10 mL) was refluxed. A solution of **19** (227 mg, 1.00 mmol) in CCl₄ (5 mL) was added to the refluxing mixture, and the mixture was further refluxed for 8 h, then cooled to room temperature and concentrated. The resulting residue was purified by column chromatography (0–10% EtOAc/hexane) to afford the title compound (82.0 mg, 36%).

¹H NMR (300 MHz, CDCl₃) δ 4.57 (s, 2H), 4.72 (s, 2H), 7.09 (m, 1H), 7.63–7.65 (m, 2H).

tert-Butyl 4-[(3-Oxo-2,3-dihydrobenzofuran-7-yl)methyl]piperazine-1-carboxylate (21). To a solution of *N*-Boc-piperazine (130 mg, 0.697 mmol) in CH₂Cl₂ (2 mL) was added dropwise a solution of **20** (72.0 mg, 0.317 mmol) in CH₂Cl₂ (1 mL) at room temperature. The mixture was stirred at room temperature for 12 h and concentrated in vacuo. The resulting residue was purified by column chromatography (0–2% MeOH/CHCl₃) to afford the title compound (105 mg, quant.).

¹H NMR (300 MHz, CDCl₃) δ 1.45 (s, 9H), 2.46 (t, *J* = 5.1 Hz, 4H), 3.45 (t, *J* = 5.1 Hz, 4H), 3.64 (s, 2H), 4.65 (s, 2H), 7.09 (t, *J* = 7.3 Hz, 1H), 7.59–7.65 (m, 2H).

(Z)-tert-Butyl 4-[(2-[(1H-Indol-3-yl)methylene]-3-oxo-2,3-dihydrobenzofuran-7-yl)methyl]piperazine-1-carboxylate (22). A mixture of **21** (79.6 mg, 0.239 mmol), 1H-indole-3-carbaldehyde (34.7 mg, 0.239 mmol), and piperidine (16.3 mg, 0.191 mmol) in MeOH (1 mL) was heated at 60 °C for 2 h, then cooled to room temperature and concentrated in vacuo. The resulting residue was purified by column chromatography (0–2% MeOH/CHCl₃) to afford the title compound (83.8 mg, 76%).

¹H NMR (300 MHz, DMSO-*d*₆) δ 1.38 (s, 9H), 2.47 (m, 4H), 3.37 (m, 4H), 3.84 (s, 2H), 7.17–7.30 (m, 3H), 7.38 (s, 1H), 7.52 (d, *J* = 8.1 Hz, 1H), 7.69–7.72 (m, 2H), 8.17 (d, *J* = 8.0 Hz, 1H), 8.26 (d, *J* = 2.2 Hz, 1H), 12.12 (br s, 1H).

(Z)-2-[(1H-Indol-3-yl)methylene]-7-(piperazin-1-ylmethyl)benzofuran-3(2H)-one (5). To a suspension of **22** (56.0 mg, 0.122 mmol) in CH₂Cl₂ (7 mL) was added 4 N HCl in dioxane (7 mL) at room temperature. The mixture was stirred at the same temperature for 2 h and concentrated in vacuo, and then 7 mL of saturated aqueous NaHCO₃ was added. The precipitated yellow powder was collected by filtration, washed with water, and dried in vacuo to afford the title compound as an orange powder (29.6 mg, 67%).

¹H NMR (300 MHz, DMSO-*d*₆) δ 2.46 (m, 4H), 2.73 (m, 4H), 3.78 (s, 2H), 7.18–7.29 (m, 3H), 7.38 (s, 1H), 7.52 (d, *J* = 8.1 Hz, 1H), 7.69 (d, *J* = 7.3 Hz, 2H), 8.19 (d, *J* = 8.1 Hz, 1H), 8.26 (s, 1H), 12.16 (br s, 1H).

HRMS (ESI⁺) calcd for (C₂₂H₂₂N₃O₂) [M + H]⁺ 360.1712; found 360.1736.

tert-Butyl 4-[(6-Methoxy-3-oxo-2,3-dihydrobenzofuran-7-yl)methyl]piperazine-1-carboxylate (23). A mixture of **16** (1.74 g, 5.00 mmol), MeOH (0.243 mL, 6.00 mmol), triphenylphosphine

(1.97 g, 7.50 mmol), and 40% diethylazodicarboxylate (DEAD) in toluene (3.27 g, 7.50 mmol) in toluene (20 mL) was stirred at 110 °C for 5 h, then cooled to room temperature and concentrated in vacuo. The resulting residue was purified by column chromatography (0–75% EtOAc/CHCl₃). The crude product obtained was further purified by column chromatography (0–50% EtOAc/hexane) to afford the title compound (790 mg, 43%).

¹H NMR (300 MHz, CDCl₃) δ 1.44 (s, 9H), 2.48 (m, 4H), 3.42 (t, *J* = 5.1 Hz, 4H), 3.70 (s, 2H), 3.93 (s, 3H), 4.64 (s, 2H), 6.70 (d, *J* = 8.8 Hz, 1H), 7.62 (d, *J* = 8.8 Hz, 1H).

tert-Butyl 4-[(6-Ethoxy-3-oxo-2,3-dihydrobenzofuran-7-yl)methyl]piperazine-1-carboxylate (24). From **16** (522 mg, 1.50 mmol) and EtOH (0.105 mL, 1.80 mmol), the title compound was obtained (158 mg, 28%) in the same manner as described for **23**.

¹H NMR (300 MHz, CDCl₃) δ 1.44–1.48 (m, 12H), 2.49 (m, 4H), 3.41 (m, 4H), 3.72 (s, 2H), 4.15 (q, *J* = 7.3 Hz, 2H), 4.64 (s, 2H), 6.67 (d, *J* = 8.8 Hz, 1H), 7.59 (d, *J* = 8.8 Hz, 1H).

tert-Butyl 4-[(3-Oxo-6-propoxy-2,3-dihydrobenzofuran-7-yl)methyl]piperazine-1-carboxylate (25). From **16** (522 mg, 1.50 mmol) and *n*-propanol (0.135 mL, 1.80 mmol), the title compound was obtained (205 mg, 35%) in the same manner as described for **23**.

¹H NMR (300 MHz, CDCl₃) δ 1.07 (t, *J* = 7.3 Hz, 3H), 1.44 (s, 9H), 1.80–1.91 (m, 2H), 2.48 (m, 4H), 3.41 (t, *J* = 5.1 Hz, 4H), 3.71 (s, 2H), 4.04 (t, *J* = 6.6 Hz, 2H), 4.64 (s, 2H), 6.67 (d, *J* = 8.8 Hz, 1H), 7.59 (d, *J* = 8.8 Hz, 1H).

tert-Butyl 4-[(6-(Benzyloxy)-3-oxo-2,3-dihydrobenzofuran-7-yl)methyl]piperazine-1-carboxylate (26). From **16** (522 mg, 1.50 mmol) and benzyl alcohol (0.186 mL, 1.80 mmol), the title compound was obtained (259 mg, 39%) in the same manner as described for **23**.

¹H NMR (300 MHz, CDCl₃) δ 1.44 (s, 9H), 2.48 (m, 4H), 3.40 (m, 4H), 3.73 (s, 2H), 4.65 (s, 2H), 5.20 (s, 2H), 6.76 (d, *J* = 8.8 Hz, 1H), 7.35–7.45 (m, 5H), 7.60 (d, *J* = 8.8 Hz, 1H).

(Z)-tert-Butyl 4-[(2-[(1H-Indol-3-yl)methylene]-6-methoxy-3-oxo-2,3-dihydrobenzofuran-7-yl)methyl]piperazine-1-carboxylate (27). A mixture of **23** (181 mg, 0.500 mmol), 1H-indole-3-carbaldehyde (72.6 mg, 0.500 mmol), and piperidine (34.1 mg, 0.400 mmol) in MeOH (2 mL) was stirred at 60 °C for 2 h, then cooled to room temperature. The precipitate was collected by filtration to afford the title compound (165 mg, 67%).

¹H NMR (300 MHz, DMSO-*d*₆) δ 1.37 (s, 9H), 2.48 (m, 4H), 3.31 (m, 4H), 3.78 (s, 2H), 3.95 (s, 3H), 7.01 (d, *J* = 8.8 Hz, 1H), 7.16–7.27 (m, 3H), 7.51 (d, *J* = 8.1 Hz, 1H), 7.73 (d, *J* = 8.8 Hz, 1H), 8.15 (d, *J* = 7.3 Hz, 1H), 8.20 (s, 1H), 12.06 (br s, 1H).

(Z)-tert-Butyl 4-[(2-[(1H-Indol-3-yl)methylene]-6-ethoxy-3-oxo-2,3-dihydrobenzofuran-7-yl)methyl]piperazine-1-carboxylate (28). From **24** (138 mg, 0.367 mmol), the title compound was obtained (137 mg, 74%) in the same manner as described for **27**.

¹H NMR (300 MHz, DMSO-*d*₆) δ 1.36–1.42 (m, 12H), 2.47 (m, 4H), 3.31 (m, 4H), 3.80 (s, 2H), 4.22 (q, *J* = 6.6 Hz, 2H), 6.98 (d, *J* = 8.8 Hz, 1H), 7.15–7.27 (m, 3H), 7.51 (d, *J* = 8.1 Hz, 1H), 7.70 (d, *J* = 8.8 Hz, 1H), 8.14 (d, *J* = 8.0 Hz, 1H), 8.20 (d, *J* = 2.9 Hz, 1H), 12.04 (br s, 1H).

(Z)-tert-Butyl 4-[(2-[(1H-Indol-3-yl)methylene]-3-oxo-6-propoxy-2,3-dihydrobenzofuran-7-yl)methyl]piperazine-1-carboxylate (29). From **25** (163 mg, 0.417 mmol), the title compound was obtained (166 mg, 77%) in the same manner as described for **27**.

¹H NMR (300 MHz, DMSO-*d*₆) δ 1.05 (t, *J* = 7.3 Hz, 3H), 1.37 (s, 9H), 1.74–1.86 (m, 2H), 2.51 (m, 4H), 3.30 (m, 4H), 3.79 (s, 2H), 4.12 (t, *J* = 5.9 Hz, 2H), 6.98 (d, *J* = 8.8 Hz, 1H), 7.18 (t, *J* = 7.3 Hz, 1H), 7.22–7.27 (m, 2H), 7.51 (d, *J* = 7.3 Hz, 1H), 7.70 (d, *J* = 8.8 Hz, 1H), 8.14 (d, *J* = 8.1 Hz, 1H), 8.19 (d, *J* = 2.9 Hz, 1H), 12.03 (br s, 1H).

(Z)-tert-Butyl 4-[(2-[(1H-Indol-3-yl)methylene]-6-(benzyloxy)-3-oxo-2,3-dihydrobenzofuran-7-yl)methyl]piperazine-1-carboxylate (30). From **26** (120 mg, 0.319 mmol), the title compound was obtained (86.4 mg, 53%) in the same manner as described for **27**.

¹H NMR (300 MHz, DMSO-*d*₆) δ 1.37 (s, 9H), 2.48 (m, 4H), 3.30 (m, 4H), 3.81 (s, 2H), 5.34 (s, 2H), 7.10 (d, *J* = 8.8 Hz, 1H), 7.16–7.27 (m, 3H), 7.34–7.46 (m, 3H), 7.50–7.55 (m, 3H), 7.72 (d, *J* = 8.8

H_z, 1H), 8.14 (d, *J* = 8.1 Hz, 1H), 8.20 (d, *J* = 2.9 Hz, 1H), 12.05 (br s, 1H).

(Z)-2-[(1H-Indol-3-yl)methylene]-6-methoxy-7-(piperazin-1-ylmethyl)benzofuran-3(2H)-one (6). To a suspension of 27 (78.3 mg, 0.160 mmol) in CH₂Cl₂ (3 mL) was added 4 N HCl in dioxane (3 mL) at room temperature. The mixture was stirred at the same temperature for 2 h and concentrated in vacuo, then 3 mL of saturated aqueous NaHCO₃ was added. The precipitated yellow powder was collected by filtration, washed with water, and dried in vacuo to afford the title compound as a yellow powder (50.0 mg, 80%).

¹H NMR (300 MHz, DMSO-*d*₆) δ 2.44 (m, 4H), 2.66 (m, 4H), 3.72 (s, 2H), 3.94 (s, 3H), 7.00 (d, *J* = 8.8 Hz, 1H), 7.17 (m, 1H), 7.20–7.26 (m, 2H), 7.50 (d, *J* = 8.0 Hz, 1H), 7.72 (d, *J* = 8.1 Hz, 1H), 8.14 (d, *J* = 8.0 Hz, 1H), 8.20 (s, 1H), 12.09 (br s, 1H).

HRMS (ESI⁺) calcd for (C₂₃H₂₄N₃O₃) [M + H]⁺ 390.1818; found 390.1845.

(Z)-2-[(1H-Indol-3-yl)methylene]-6-ethoxy-7-(piperazin-1-ylmethyl)benzofuran-3(2H)-one (7). From 28 (106 mg, 0.210 mmol), the title compound was obtained (65.3 mg, 77%) in the same manner as described for 6.

¹H NMR (300 MHz, DMSO-*d*₆) δ 1.39 (t, *J* = 7.3 Hz, 3H), 2.46 (m, 4H), 2.67 (m, 4H), 3.74 (s, 2H), 4.20 (q, *J* = 7.3 Hz, 2H), 6.97 (d, *J* = 8.8 Hz, 1H), 7.17 (t, *J* = 7.3 Hz, 1H), 7.21–7.26 (m, 2H), 7.50 (d, *J* = 7.3 Hz, 1H), 7.68 (d, *J* = 8.8 Hz, 1H), 8.15 (d, *J* = 7.3 Hz, 1H), 8.19 (s, 1H), 12.08 (br s, 1H).

HRMS (ESI⁺) calcd for (C₂₄H₂₆N₃O₃) [M + H]⁺ 404.1974; found 404.1968.

(Z)-2-[(1H-Indol-3-yl)methylene]-7-(piperazin-1-ylmethyl)-6-propoxybenzofuran-3(2H)-one (8). From 29 (70.5 mg, 0.136 mmol), the title compound was obtained (30.6 mg, 53%) in the same manner as described for 6.

¹H NMR (300 MHz, DMSO-*d*₆) δ 1.05 (t, *J* = 7.3 Hz, 3H), 1.73–1.85 (m, 2H), 2.46 (m, 4H), 2.66 (m, 4H), 3.72 (s, 2H), 4.11 (t, *J* = 5.9 Hz, 2H), 6.97 (d, *J* = 8.8 Hz, 1H), 7.17 (t, *J* = 7.3 Hz, 1H), 7.21–7.26 (m, 2H), 7.50 (d, *J* = 8.1 Hz, 1H), 7.68 (d, *J* = 8.8 Hz, 1H), 8.15 (d, *J* = 8.1 Hz, 1H), 8.19 (s, 1H), 12.08 (br s, 1H).

HRMS (ESI⁺) calcd for (C₂₅H₂₈N₃O₃) [M + H]⁺ 418.2131; found 418.2175.

(Z)-2-[(1H-Indol-3-yl)methylene]-6-(benzyloxy)-7-(piperazin-1-ylmethyl)benzofuran-3(2H)-one (9). From 30 (123 mg, 0.217 mmol), the title compound was obtained (72.0 mg, 71%) in the same manner as described for 6.

¹H NMR (300 MHz, DMSO-*d*₆) δ 2.46 (m, 4H), 2.68 (m, 4H), 3.76 (s, 2H), 5.33 (s, 2H), 7.09 (d, *J* = 8.8 Hz, 1H), 7.16–7.27 (m, 3H), 7.33–7.45 (m, 3H), 7.49–7.56 (m, 3H), 7.71 (d, *J* = 8.8 Hz, 1H), 8.16 (d, *J* = 8.1 Hz, 1H), 8.20 (s, 1H), 12.08 (br s, 1H).

HRMS (ESI⁺) calcd for (C₂₉H₂₈N₃O₃) [M + H]⁺ 466.2131; found 466.2120.

(Z)-tert-Butyl 4-({2-[(1H-Pyrrolo[2,3-*b*]pyridin-3-yl)methylene]-6-methoxy-3-oxo-2,3-dihydrobenzofuran-7-yl)methyl)piperazine-1-carboxylate (31). A mixture of 23 (478 mg, 1.32 mmol), 7-azaindole-3-carbaldehyde (193 mg, 1.32 mmol), and piperidine (90.3 mg, 1.06 mmol) in MeOH (5 mL) was stirred at 60 °C for 2 h, then cooled to room temperature. The precipitate was collected by filtration to afford the title compound (220 mg, 33%).

¹H NMR (300 MHz, DMSO-*d*₆) δ 1.36 (s, 9H), 2.46 (m, 4H), 3.30 (m, 4H), 3.76 (s, 2H), 3.95 (s, 3H), 7.02 (d, *J* = 8.8 Hz, 1H), 7.23 (dd, *J* = 4.4 Hz, 8.0 Hz, 1H), 7.24 (s, 1H), 7.74 (d, *J* = 8.8 Hz, 1H), 8.27 (s, 1H), 8.35 (dd, *J* = 1.5 Hz, 4.4 Hz, 1H), 8.66 (dd, *J* = 1.5 Hz, 8.0 Hz, 1H), 12.45 (br s, 1H).

(Z)-tert-Butyl 4-({2-[(1H-Pyrrolo[2,3-*c*]pyridin-3-yl)methylene]-6-methoxy-3-oxo-2,3-dihydrobenzofuran-7-yl)methyl)piperazine-1-carboxylate (32). From 23 (61.6 mg, 0.170 mmol) and 6-azaindole-3-carbaldehyde (24.8 mg, 0.170 mmol), the title compound was obtained (68.6 mg, 82%) in the same manner as described for 31.

¹H NMR (300 MHz, DMSO-*d*₆) δ 1.36 (s, 9H), 2.47 (m, 4H), 3.30 (m, 4H), 3.78 (s, 2H), 3.95 (s, 3H), 7.02 (d, *J* = 8.8 Hz, 1H), 7.26 (s, 1H), 7.74 (d, *J* = 8.8 Hz, 1H), 8.17 (d, *J* = 5.9 Hz, 1H), 8.26 (d, *J* = 5.9 Hz, 1H), 8.35 (s, 1H), 8.85 (s, 1H), 12.44 (br s, 1H).

(Z)-tert-Butyl 4-({2-[(1H-Pyrrolo[3,2-*c*]pyridin-3-yl)methylene]-6-methoxy-3-oxo-2,3-dihydrobenzofuran-7-yl)methyl)piperazine-1-carboxylate (33). From 23 (46.8 mg, 0.129 mmol) and 5-azaindole-3-carbaldehyde (18.8 mg, 0.129 mmol), the title compound was obtained (51.5 mg, 81%) in the same manner as described for 31.

¹H NMR (300 MHz, DMSO-*d*₆) δ 1.36 (s, 9H), 2.47 (m, 4H), 3.30 (m, 4H), 3.76 (s, 2H), 3.95 (s, 3H), 7.03 (d, *J* = 8.8 Hz, 1H), 7.29 (s, 1H), 7.48 (d, *J* = 5.9 Hz, 1H), 7.75 (d, *J* = 8.8 Hz, 1H), 8.21 (s, 1H), 8.32 (d, *J* = 5.9 Hz, 1H), 9.54 (s, 1H), 12.29 (br s, 1H).

(Z)-tert-Butyl 4-({2-[(1H-Pyrrolo[3,2-*b*]pyridin-3-yl)methylene]-6-methoxy-3-oxo-2,3-dihydrobenzofuran-7-yl)methyl)piperazine-1-carboxylate (34). From 23 (49.7 mg, 0.137 mmol) and 4-azaindole-3-carbaldehyde (20.0 mg, 0.137 mmol), the title compound was obtained (49.6 mg, 73%) in the same manner as described for 31.

¹H NMR (300 MHz, DMSO-*d*₆) δ 1.36 (s, 9H), 2.47 (m, 4H), 3.30 (m, 4H), 3.80 (s, 2H), 3.95 (s, 3H), 7.02 (d, *J* = 8.8 Hz, 1H), 7.26 (dd, *J* = 4.4 Hz, 8.0 Hz, 1H), 7.31 (s, 1H), 7.73 (d, *J* = 8.8 Hz, 1H), 7.92 (dd, *J* = 1.5 Hz, 8.0 Hz, 1H), 8.39 (s, 1H), 8.48 (dd, *J* = 1.5 Hz, 4.4 Hz, 1H), 12.00 (br s, 1H).

(Z)-tert-Butyl 4-({2-[(1H-Indazol-3-yl)methylene]-6-methoxy-3-oxo-2,3-dihydrobenzofuran-7-yl)methyl)piperazine-1-carboxylate (35). From 23 (181 mg, 0.500 mmol) and 1H-indazole-3-carbaldehyde (73.1 mg, 0.500 mmol), the title compound was obtained (171 mg, 69%) in the same manner as described for 31.

¹H NMR (300 MHz, DMSO-*d*₆) δ 1.35 (s, 9H), 2.46 (m, 4H), 3.29 (m, 4H), 3.74 (s, 2H), 3.97 (s, 3H), 7.05–7.08 (m, 2H), 7.26 (t, *J* = 7.3 Hz, 1H), 7.47 (t, *J* = 7.3 Hz, 1H), 7.65 (d, *J* = 8.8 Hz, 1H), 7.80 (d, *J* = 8.8 Hz, 1H), 8.60 (d, *J* = 8.0 Hz, 1H), 13.86 (br s, 1H).

(Z)-2-[(1H-Pyrrolo[2,3-*b*]pyridin-3-yl)methylene]-6-methoxy-7-(piperazin-1-ylmethyl)benzofuran-3(2H)-one (10). To a suspension of 31 (147 mg, 0.300 mmol) in CH₂Cl₂ (14 mL) was added 4 N HCl in dioxane (14 mL) at room temperature. The mixture was stirred at the same temperature for 2 h and concentrated in vacuo, and then 14 mL of saturated aqueous NaHCO₃ was added to the residue. The mixture was extracted with EtOAc (×5), and the combined organic layers were dried over Na₂SO₄. Evaporation of the solvent afforded the title compound (14.6 mg, 12%).

¹H NMR (300 MHz, DMSO-*d*₆) δ 2.46 (m, 4H), 2.72 (m, 4H), 3.72 (s, 2H), 3.95 (s, 3H), 7.02 (d, *J* = 8.8 Hz, 1H), 7.20–7.24 (m, 2H), 7.74 (d, *J* = 8.8 Hz, 1H), 8.27 (s, 1H), 8.35 (d, *J* = 4.4 Hz, 1H), 8.68 (d, *J* = 8.0 Hz, 1H).

HRMS (ESI⁺) calcd for (C₂₂H₂₃N₄O₃) [M + H]⁺ 391.1770; found 391.1783.

(Z)-2-[(1H-Pyrrolo[2,3-*c*]pyridin-3-yl)methylene]-6-methoxy-7-(piperazin-1-ylmethyl)benzofuran-3(2H)-one (11). To a suspension of 32 (52.1 mg, 0.106 mmol) in CH₂Cl₂ (5 mL) was added 4 N HCl in dioxane (5 mL) at room temperature. The mixture was stirred at the same temperature for 2 h and concentrated in vacuo, and then 5 mL of saturated aqueous NaHCO₃ was added to the residue. The mixture was extracted with CHCl₃ (×5), and the combined organic layers were dried over Na₂SO₄. Evaporation of the solvent afforded the title compound (13.1 mg, 31%).

¹H NMR (300 MHz, DMSO-*d*₆) δ 2.54 (m, 4H), 2.81 (m, 4H), 3.78 (s, 2H), 3.96 (s, 3H), 7.03 (d, *J* = 8.8 Hz, 1H), 7.27 (s, 1H), 7.75 (d, *J* = 8.8 Hz, 1H), 8.20 (d, *J* = 5.1 Hz, 1H), 8.27 (d, *J* = 5.1 Hz, 1H), 8.36 (s, 1H), 8.86 (s, 1H).

HRMS (ESI⁺) calcd for (C₂₂H₂₃N₄O₃) [M + H]⁺ 391.1770; found 391.1723.

(Z)-2-[(1H-Pyrrolo[3,2-*c*]pyridin-3-yl)methylene]-6-methoxy-7-(piperazin-1-ylmethyl)benzofuran-3(2H)-one (12). From 33 (36.9 mg, 0.0752 mmol), the title compound was obtained (18.2 mg, 61%) in the same manner as described for 11.

¹H NMR (300 MHz, DMSO-*d*₆) δ 2.55 (m, 4H), 2.71 (m, 4H), 3.73 (s, 2H), 3.96 (s, 3H), 7.03 (d, *J* = 8.8 Hz, 1H), 7.30 (s, 1H), 7.48 (d, *J* = 5.9 Hz, 1H), 7.75 (d, *J* = 8.8 Hz, 1H), 8.23 (s, 1H), 8.32 (d, *J* = 5.9 Hz, 1H), 9.52 (s, 1H).

HRMS (ESI⁺) calcd for (C₂₂H₂₃N₄O₃) [M + H]⁺ 391.1770; found 391.1785.

(Z)-2-[(1*H*-Pyrrolo[3,2-*b*]pyridin-3-yl)methylene]-6-methoxy-7-(piperazin-1-ylmethyl)benzofuran-3(2*H*)-one (**13**). From **34** (33.0 mg, 0.0673 mmol), the title compound was obtained (19.9 mg, 75%) in the same manner as described for **10**.

¹H NMR (300 MHz, DMSO-*d*₆) δ 2.45 (m, 4H), 2.66 (m, 4H), 3.74 (s, 2H), 3.94 (s, 3H), 7.01 (d, *J* = 8.8 Hz, 1H), 7.26 (dd, *J* = 4.4 Hz, 8.1 Hz, 1H), 7.31 (s, 1H), 7.72 (d, *J* = 8.8 Hz, 1H), 7.91 (dd, *J* = 1.5 Hz, 8.1 Hz, 1H), 8.39 (s, 1H), 8.48 (dd, *J* = 1.5 Hz, 4.4 Hz, 1H).

HRMS (ESI⁺) calcd for (C₂₂H₂₃N₄O₃) [M + H]⁺ 391.1770; found 391.1770.

(Z)-2-[(1*H*-Indazol-3-yl)methylene]-6-methoxy-7-(piperazin-1-ylmethyl)benzofuran-3(2*H*)-one (**14**). From **35** (125 mg, 0.255 mmol), the title compound was obtained (77.7 mg, 78%) in the same manner as described for **10**.

¹H NMR (400 MHz, DMSO-*d*₆) δ 2.44 (m, 4H), 2.67 (m, 4H), 3.68 (s, 2H), 3.96 (s, 3H), 7.04 (d, *J* = 8.8 Hz, 1H), 7.07 (s, 1H), 7.25 (t, *J* = 7.3 Hz, 1H), 7.47 (m, 1H), 7.64 (d, *J* = 8.8 Hz, 1H), 7.78 (d, *J* = 8.8 Hz, 1H), 8.62 (d, *J* = 8.8 Hz, 1H).

HRMS (ESI⁺) calcd for (C₂₂H₂₃N₄O₃) [M + H]⁺ 391.1770; found 391.1740.

6-Azaindole-3-carbaldehyde. A mixture of 6-azaindole (118 mg, 1.00 mmol), hexamethylenetetramine (210 mg, 1.50 mmol), and acetic acid (0.6 mL) in H₂O (1.2 mL) was heated at 120 °C for 6 h, then cooled to room temperature and basified by the addition of saturated aqueous NaHCO₃. After extraction with AcOEt (×3), the combined organic layers were washed with brine, dried over MgSO₄, and concentrated. The resulting residue was washed with CH₂Cl₂ to afford the title compound (47.9 mg, 32%).

¹H NMR (300 MHz, DMSO-*d*₆) δ 7.99 (d, *J* = 5.9 Hz, 1H), 8.32 (d, *J* = 5.9 Hz, 1H), 8.51 (s, 1H), 8.87 (s, 1H), 10.00 (s, 1H), 12.57 (br s, 1H).

PIM1 Inhibition Assay. Enzyme inhibition was examined by means of electrophoretic mobility shift assay. An aqueous suspension containing 1.5 μM FL-Peptide 20, 5-FAM-RSRHSSYPAGT-CONH₂ (Caliper Life Science, Hopkinton, MA), 30 μM ATP, 33 ng/mL PIM1,⁴³ 50 mM Hepes (pH 7.4), 10 mM MgCl₂, 1 mM DTT, 1% Protease Inhibitor Cocktail Set V (Merck, Darmstadt, Germany), 1% Phosphatase Inhibitor Cocktail Set III (Merck), 0.01% Brij-35, and a test compound (in 5% DMSO) was incubated for 2 h at room temperature, and the reaction was stopped by addition of 140 mM EDTA. Phosphorylated and unphosphorylated peptides obtained were separated and detected with a Lab-Chip EZ Reader II (Caliper Life Science).

Kinase Selectivity Assay. Kinase selectivity was evaluated against a panel of 20 protein tyrosine kinases and 30 serine/threonine kinases at CarnaBiosciences (<http://www.carnabio.com>). The ATP concentration used was approximately equal to the *K*_m value for each kinase. Each compound was tested at a concentration 50-fold higher than its IC₅₀ value in the PIM1-inhibitory assay (**1**, 22500 nM; **3**, 600 nM; **6**, 250 nM; **10**, 200 nM; **14**, 300 nM). For these experiments, the IC₅₀ values for PIM1 of each compound were determined at CarnaBiosciences. Kinase inhibition was examined by electrophoretic mobility shift assay except for JNK2, MAP2K1, MLK1, and RAF1, which were examined by ELISA.

Cell Growth Inhibition Assay. MV4–11 (ATCC, Manassas, VA) and WI-38 (RIKEN BioResource Center, Japan) cells were cultured in Iscove's modified Dulbecco's medium (Invitrogen, Carlsbad, CA) containing 10% fetal bovine serum (FBS, Invitrogen) and in minimum essential medium (Invitrogen) containing 10% FBS, respectively, at 37 °C in 5% CO₂. The aqueous suspension containing MV4–11 (2 × 10⁵ cells/mL) or WI-38 (3 × 10⁴ cells/mL) was precultured for 24 h, followed by incubation for 48 h in the presence of the test compound (in 0.5% DMSO). Cell growth inhibition was measured with a Cell Counting Kit-8 (Dojindo, Japan) according to the manufacturer's instruction. Absorbance at 450 nm was monitored with PHERAstar (BMG Labtech, Germany).

Western Blotting. MV4–11 cells precultured for 24 h were incubated in the presence of the test compound (in 0.5% DMSO) for 1 h. The cells were washed with PBS and dispersed in β-ME Sample Treatment for Tris SDS (Cosmobio, Japan). The suspension was

boiled for 5 min, and the lysates were applied to 12.5% polyacrylamide gels (Cosmobio) and separated by SDS polyacrylamide gel electrophoresis. The gels were blotted onto polyvinylidene difluoride membrane (BIO-RAD, Hercules, CA), and the membrane was incubated with the primary antibody, Total BAD, Phospho-BAD (Ser-112), or Phospho-BAD (Ser-136) (Cell Signaling Technology, Danvers, MA) for 16 h at 4 °C. The membrane was washed with TBS-T and incubated with Anti-Rabbit IgG HRP conjugates (GE Healthcare, Buckinghamshire, UK) for 1 h at room temperature. Chemiluminescence signals of protein obtained on addition of ECL Plus (GE Healthcare) reagent were analyzed with an ImageQuant LAS 4000 (GE Healthcare).

Apoptosis and Cell-Cycle Analysis. MV4–11 was maintained in Iscove's modified Dulbecco's medium with 10% FBS and penicillin (5000 U/mL)–streptomycin (5 mg/mL) (Sigma) at 37 °C in 5% CO₂. MV4–11 cells (1 × 10⁵ cells/mL) were cultured with the compounds for 48 h and then harvested. Cells were stained with ApoAlert AnnexinV (Clontech 630109) for apoptosis analysis and Cycle TEST PLUS DNA Reagent Kit (Becton, Dickinson) for cell cycle analysis according to the manufacturers' instructions. Cells were analyzed with a flow cytometer (CaliburTM, Becton, Dickinson and Company, Franklin Lakes, NJ). Data analysis was performed using FlowJo software (Tree Star, Ashland, Oregon).

ADMET Study. Metabolic stability assay with liver microsomes and hepatocytes, CYP inhibition assay, and hERG inhibition assay were carried out at Cerep (<http://www.cerep.fr/Cerep/Users/>).

PIM1 Crystallization. The kinase domain (residues 29–313) of human PIM-1 was synthesized in an *Escherichia coli* cell-free system, using the dialysis method.^{66–68} The protein was purified as described previously⁴³ and dialyzed against buffer containing 20 mM Tris-HCl (pH 8.0), 200 mM NaCl, 2 mM CaCl₂, 2 mM MgCl₂, and 5 mM DTT, then concentrated to 12 mg/mL. Crystallization was carried out under conditions previously reported by Jacobs et al.⁶⁹ Briefly, the protein was crystallized by the hanging drop vapor diffusion method at 20 °C, and the compound was allowed to soak into the crystal for 24 h. Data for the PIM1-**14** complex were collected on beamline BL26B2, SPring-8, Harima, Japan. The crystals belonged to the spacegroup P65, with cell dimensions of *a*, *b*, *c* = 98.28, 98.28, 80.64, respectively, and α = β = 90° and γ = 120°. Statistics are presented in Table S2, Supporting Information.

PIM1 Structure Solution. The resolution was 2.08 Å. The data were processed and integrated with the Mosflm⁷⁰ program and scaled with the Scala⁷¹ program. Molecular replacement was performed with Phaser,⁷² using PDB code 3A99 as the search model, with the peptide removed. There is one molecule in the asymmetric unit. Refinement was performed using Refmac (CCP4),⁷³ and model building was accomplished with COOT.⁷⁴ The electron density of the compound was immediately evident in the *F*_o – *F*_c and 2*F*_o – *F*_c maps, and the compound was built using Monomer Library Sketcher (CCP4). The ligand was fitted with 100% occupancy and refined with an average *B*-factor of 24.4. The average temperature factor for the protein is 28.26 for the main chain and 30.16 for the side chains. The final *R*-factor and *R*_{free} values were 17.35 and 20.03, respectively. Statistics for the complex are presented in Table S2, Supporting Information.

■ ASSOCIATED CONTENT

📄 Supporting Information

Raw data of the kinase selectivity study and crystallographic data collection and refinement statistics. This material is available free of charge via the Internet at <http://pubs.acs.org>.

Accession Codes

The atomic coordinates and structure factors have been deposited in the Protein Data Bank, www.rcsb.org (PDB ID codes 3UMW and 3UMX).

AUTHOR INFORMATION

Corresponding Author

*Phone: +81-3-5841-4850. Fax: +81-3-5841-4855. E-mail: tlong@mol.f.u-tokyo.ac.jp. Address: Graduate School of Pharmaceutical Sciences, The University of Tokyo, 7-3-1 Hongo, Bunkyo-ku, Tokyo 113-0033, Japan.

Notes

The authors declare no competing financial interest.

ACKNOWLEDGMENTS

This work was supported by the Targeted Proteins Research Program from the Ministry of Education, Culture, Sports, Science and Technology of Japan. L.P. is supported by a National Health and Medical Research Council of Australia (NHMRC). C.J. Martin Overseas Postdoctoral Fellowship. We thank Mio Inoue, Noboru Ohsawa, and Tahako Terada for preparation of the PIM1 expression plasmid. We also thank the staff at beamline BL26, Spring-8 Harima, Japan, for their assistance with crystallographic data collection.

ABBREVIATIONS USED

PIM, proviral integration site in Moloney murine leukemia virus; BAD, Bcl-2 antagonist of cell death; CDC25, cell division cycle 25; CXCR4, CXC chemokine receptor 4; BCRP, breast cancer resistance protein; FLT3, Fms-like tyrosine kinase 3; PDGF α , platelet-derived growth factor receptor α ; SYK, spleen tyrosine kinase; GSK3 β , glycogen synthase kinase 3 β ; EGFR, epidermal growth factor receptor; KDR, kinase insert domain receptor; MLK1, mixed-lineage kinase 1; MST1, mammalian homologue Ste20-like kinase 1; DAPK1, death-associated protein kinase 1; PKC α , protein kinase C α ; PKD2, protein kinase D2; ROCK1, Rho-associated, coiled-coil containing protein kinase 1

REFERENCES

- Brault, L.; Gasser, C.; Bracher, F.; Huber, K.; Knapp, S.; Schwaller, J. PIM serine/threonine kinases in the pathogenesis and therapy of hematologic malignancies and solid cancers. *Haematologica* **2010**, *95*, 1004–1015.
- Magnuson, N. S.; Wang, Z.; Ding, G.; Reeves, R. Why target PIM1 for cancer diagnosis and treatment? *Future Oncol.* **2010**, *6*, 1461–1478.
- Amson, R.; Sigaux, F.; Przedborski, S.; Flandrin, G.; Givol, D.; Telerman, A. The human protooncogene product p33pim is expressed during fetal hematopoiesis and in diverse leukemias. *Proc. Natl. Acad. Sci. U.S.A.* **1989**, *86*, 8857–8861.
- Dhanasekaran, S. M.; Barrette, T. R.; Ghosh, D.; Shah, R.; Varambally, S.; Kurachi, K.; Pienta, K. J.; Rubin, M. A.; Chinnaiyan, A. M. Delineation of prognostic biomarkers in prostate cancer. *Nature* **2001**, *412*, 822–826.
- Lilly, M.; Kraft, A. Enforced expression of the M_r 33,000 Pim-1 kinase enhances factor-independent survival and inhibits apoptosis in murine myeloid cells. *Cancer Res.* **1997**, *57*, 5348–5355.
- van Lohuizen, M.; Verbeek, S.; Krimpenfort, P.; Domen, J.; Saris, C.; Radaszkiewicz, T.; Berns, A. Predisposition to lymphomagenesis in *pim-1* transgenic mice: cooperation with *c-myc* and *N-myc* in murine leukemia virus-induced tumors. *Cell* **1989**, *56*, 673–682.
- Breuer, M.; Slebos, R.; Verbeek, S.; van Lohuizen, M.; Wientjens, E.; Berns, A. Very high frequency of lymphoma induction by a chemical carcinogen in *pim-1* transgenic mice. *Nature* **1989**, *340*, 61–63.
- Aho, T. L.; Sandholm, J.; Peltola, K. J.; Mankonen, H. P.; Lilly, M.; Koskinen, P. J. Pim-1 kinase promotes inactivation of the pro-apoptotic Bad protein by phosphorylating it on the Ser¹¹² gatekeeper site. *FEBS Lett.* **2004**, *571*, 43–49.

(9) Zhang, Y.; Wang, Z.; Li, X.; Magnuson, N. S. Pim kinase-dependent inhibition of *c-Myc* degradation. *Oncogene* **2008**, *27*, 4809–4819.

(10) Zippo, A.; De Robertis, A.; Serafini, R.; Oliviero, S. PIM1-dependent phosphorylation of histone H3 at serine 10 is required for MYC-dependent transcriptional activation and oncogenic transformation. *Nature Cell Biol.* **2007**, *9*, 932–944.

(11) Zhang, Y.; Wang, Z.; Magnuson, N. S. Pim-1 kinase-dependent phosphorylation of p21^{Cip1/WAF1} regulates its stability and cellular localization in H1299 cells. *Mol. Cancer Res.* **2007**, *5*, 909–922.

(12) Morishita, D.; Katayama, R.; Sekimizu, K.; Tsuruo, T.; Fujita, N. Pim kinases promote cell cycle progression by phosphorylating and down-regulating p27^{Kip1} at the transcriptional and posttranscriptional levels. *Cancer Res.* **2008**, *68*, 5076–5085.

(13) Mochizuki, T.; Kitanaka, C.; Noguchi, K.; Muramatsu, T.; Asai, A.; Kuchino, Y. Physical and functional interactions between Pim-1 kinase and Cdc25A phosphatase. *J. Biol. Chem.* **1999**, *274*, 18659–18666.

(14) Bachmann, M.; Kosan, C.; Xing, P. X.; Montenarh, M.; Hoffmann, I.; Mörröy, T. The oncogenic serine/threonine kinase Pim-1 directly phosphorylates and activates the G2/M specific phosphatase Cdc25C. *Int. J. Biochem. Cell Biol.* **2006**, *38*, 430–443.

(15) Grundler, R.; Brault, L.; Gasser, C.; Bullock, A. N.; Dechow, T.; Woetzel, S.; Pogacic, V.; Villa, A.; Ehret, S.; Berridge, G.; Spoo, A.; Dierks, C.; Biondi, A.; Knapp, S.; Duyster, J.; Schwaller, J. Dissection of PIM serine/threonine kinases in FLT3-ITD-induced leukemogenesis reveals PIM1 as regulator of CXCL12-CXCR4-mediated homing and migration. *J. Exp. Med.* **2009**, *206*, 1957–1970.

(16) Xie, Y.; Burcu, M.; Linn, D. E.; Qiu, Y.; Baer, M. R. Pim-1 kinase protects p-glycoprotein from degradation and enables its glycosylation and cell surface expression. *Mol. Pharmacol.* **2010**, *78*, 310–318.

(17) Xie, Y.; Xu, K.; Linn, D. E.; Yang, X.; Guo, Z.; Shimelis, H.; Nakanishi, T.; Ross, D. D.; Chen, H.; Fazli, L.; Gleave, M. E.; Qiu, Y. The 44-kDa Pim-1 kinase phosphorylates BCRP/ABCG2 and thereby promotes its multimerization and drug-resistant activity in human prostate cancer cells. *J. Biol. Chem.* **2008**, *283*, 3349–3356.

(18) Laird, P. W.; van der Lugt, N. M. T.; Clarke, A.; Domen, J.; Linders, K.; McWhir, J.; Berns, A.; Hooper, M. In vivo analysis of Pim-1 deficiency. *Nucleic Acids Res.* **1993**, *21*, 4750–4755.

(19) Morwick, T. Pim kinase inhibitors: a survey of the patent literature. *Expert Opin. Ther. Pat.* **2010**, *20*, 193–212.

(20) Bullock, A. N.; Debreczeni, J. É.; Fedorov, O. Y.; Nelson, A.; Marsden, B. D.; Knapp, S. Structural basis of inhibitor specificity of the human protooncogene proviral insertion site in moloney murine leukemia virus (PIM-1) kinase. *J. Med. Chem.* **2005**, *48*, 7604–7614.

(21) Pogacic, V.; Bullock, A. N.; Fedorov, O.; Filippakopoulos, P.; Gasser, C.; Biondi, A.; Meyer-Monard, S.; Knapp, S.; Schwaller, J. Structural analysis identifies imidazo[1,2-*b*]pyridazines as PIM kinase inhibitors with in vitro antileukemic activity. *Cancer Res.* **2007**, *67*, 6916–6924.

(22) Chen, L. S.; Redkar, S.; Bearss, D.; Wierda, W. G.; Gandhi, V. Pim kinase inhibitor, SGI-1776, induces apoptosis in chronic lymphocytic leukemia cells. *Blood* **2009**, *114*, 4150–4157.

(23) Mumenthaler, S. M.; Ng, P. Y. B.; Hodge, A.; Bearss, D.; Berk, G.; Kanekal, S.; Redkar, S.; Taverna, P.; Agus, D. B.; Jain, A. Pharmacologic inhibition of Pim kinases alters prostate cancer cell growth and resensitizes chemoresistant cells to taxanes. *Mol. Cancer Ther.* **2009**, *8*, 2882–2893.

(24) Chen, L. S.; Redkar, S.; Taverna, P.; Cortes, J. E.; Gandhi, V. Mechanism of cytotoxicity to Pim kinase inhibitor, SGI-1776, in acute myeloid leukemia. *Blood* **2011**, *118*, 693–702.

(25) Debreczeni, J. É.; Bullock, A. N.; Atilla, G. E.; Williams, D. S.; Bregman, H.; Knapp, S.; Meggers, E. Ruthenium half-sandwich complexes bound to protein kinase Pim-1. *Angew. Chem., Int. Ed. Engl.* **2006**, *45*, 1580–1585.

(26) Cheney, I. W.; Yan, S.; Appleby, T.; Walker, H.; Vo, T.; Yao, N.; Hamatake, R.; Hong, Z.; Wu, J. Z. Identification and structure-activity relationships of substituted pyridones as inhibitors of Pim-1 kinase. *Bioorg. Med. Chem. Lett.* **2007**, *17*, 1679–1683.

- (27) Tong, Y.; Stewart, K. D.; Thomas, S.; Przytulinska, M.; Johnson, E. F.; Klinghofer, V.; Levenson, J.; McCall, O.; Soni, N. B.; Luo, Y.; Lin, N.-H.; Sowin, T. J.; Giranda, V. L.; Penning, T. D. Isoxazolo[3,4-*b*]quinoline-3,4(1*H*,9*H*)-diones as unique, potent and selective inhibitors for Pim-1 and Pim-2 kinases: chemistry, biological activities, and molecular modeling. *Bioorg. Med. Chem. Lett.* **2008**, *18*, 5206–5208.
- (28) Xia, Z.; Knaak, C.; Ma, J.; Beharry, Z. M.; McInnes, C.; Wang, W.; Kraft, A. S.; Smith, C. D. Synthesis and evaluation of novel inhibitors of Pim-1 and Pim-2 protein kinases. *J. Med. Chem.* **2009**, *52*, 74–86.
- (29) Beharry, Z.; Zemska, M.; Mahajan, S.; Zhang, F.; Ma, J.; Xia, Z.; Lilly, M.; Smith, C. D.; Kraft, A. S. Novel benzylidene-thiazolidine-2,4-diones inhibit Pim protein kinase activity and induce cell cycle arrest in leukemia and prostate cancer cells. *Mol. Cancer Ther.* **2009**, *8*, 1473–1483.
- (30) Grey, R.; Pierce, A. C.; Bemis, G. W.; Jacobs, M. D.; Moody, C. S.; Jajoo, R.; Mohal, N.; Green, J. Structure-based design of 3-aryl-6-amino-triazolo[4,3-*b*]pyridazine inhibitors of Pim-1 kinase. *Bioorg. Med. Chem. Lett.* **2009**, *19*, 3019–3022.
- (31) Qian, K.; Wang, L.; Cywin, C. L.; Farmer, B. T., II; Hickey, E.; Homon, C.; Jakes, S.; Kashem, M. A.; Lee, G.; Leonard, S.; Li, J.; Magboo, R.; Mao, W.; Pack, E.; Peng, C.; Prokopowicz, A., III; Welzel, M.; Wolak, J.; Morwick, T. Hit to lead account of the discovery of a new class of inhibitors of Pim kinases and crystallographic studies revealing an unusual kinase binding mode. *J. Med. Chem.* **2009**, *52*, 1814–1827.
- (32) Akué-Gédu, R.; Rossignol, E.; Azzaro, S.; Knapp, S.; Filippakopoulos, P.; Bullock, A. N.; Bain, J.; Cohen, P.; Prudhomme, M.; Anizon, F.; Moreau, P. Synthesis, kinase inhibitory potencies, and in vitro antiproliferative evaluation of new Pim kinase inhibitors. *J. Med. Chem.* **2009**, *52*, 6369–6381.
- (33) Tao, Z.-F.; Hasvold, L. A.; Levenson, J. D.; Han, E. K.; Guan, R.; Johnson, E. F.; Stoll, V. S.; Stewart, K. D.; Stamper, G.; Soni, N.; Bouska, J. J.; Luo, Y.; Sowin, T. J.; Lin, N.-H.; Giranda, V. S.; Rosenberg, S. H.; Penning, T. D. Discovery of 3*H*-benzo[4,5]thieno[3,2-*d*]pyrimidin-4-ones as potent, highly selective, and orally bioavailable inhibitors of the human protooncogene proviral insertion site in moloney murine leukemia virus (PIM) kinases. *J. Med. Chem.* **2009**, *52*, 6621–6636.
- (34) Ren, J.-X.; Li, L.-L.; Zheng, R.-L.; Xie, H.-Z.; Cao, Z.-X.; Feng, S.; Pan, Y.-L.; Chen, X.; Wei, Y.-Q.; Yang, S.-Y. Discovery of novel Pim-1 kinase inhibitors by a hierarchical multistage virtual screening approach based on SVM model, pharmacophore, and molecular docking. *J. Chem. Inf. Model.* **2011**, *51*, 1364–1375.
- (35) Xiang, Y.; Hirth, B.; Asmussen, G.; Biemann, H.-P.; Bishop, K. A.; Good, A.; Fitzgerald, M.; Gladysheva, T.; Jain, A.; Jancsics, K.; Liu, J.; Metz, M.; Papoulis, A.; Skerlj, R.; Stepp, J. D.; Wei, R. R. The discovery of novel benzofuran-2-carboxylic acids as potent Pim-1 inhibitors. *Bioorg. Med. Chem. Lett.* **2011**, *21*, 3050–3056.
- (36) Nishiguchi, G. A.; Atallah, G.; Bellamacina, C.; Burger, M. T.; Ding, Y.; Feucht, P. H.; Garcia, P. D.; Han, W.; Klivansky, L.; Lindvall, M. Discovery of novel 3,5-disubstituted indole derivatives as potent inhibitors of Pim-1, Pim-2, and Pim-3 kinases. *Bioorg. Med. Chem. Lett.* **2011**, *21*, 6366–6369.
- (37) Pierre, F.; Stefan, E.; Nédellec, A.-S.; Chevrel, M.-C.; Regan, C. F.; Siddiqui-Jain, A.; Macalino, D.; Streiner, N.; Drygin, D.; Haddach, M.; O'Brien, S. E.; Anderes, K.; Ryckman, D. M. 7-(4*H*-1,2,4-Triazol-3-yl)benzo[*c*][2,6]naphthyridines: a novel class of Pim kinase inhibitors with potent cell antiproliferative activity. *Bioorg. Med. Chem. Lett.* **2011**, *21*, 6687–6692.
- (38) Huber, K.; Brault, L.; Fedorov, O.; Gasser, C.; Filippakopoulos, P.; Bullock, A. N.; Fabbro, D.; Trappe, J.; Schwaller, J.; Knapp, S.; Bracher, F. 7,8-Dichloro-1-oxo- β -carboline as a versatile scaffold for the development of potent and selective kinase inhibitors with unusual binding modes. *J. Med. Chem.* **2012**, *55*, 403–413.
- (39) Haddach, M.; Michaux, J.; Schwaeb, M. K.; Pierre, F.; O'Brien, S. E.; Borsan, C.; Tran, J.; Raffaele, N.; Ravula, S.; Drygin, D.; Siddiqui-Jain, A.; Darjania, L.; Stansfield, R.; Proffitt, C.; Macalino, D.; Streiner, N.; Bliesath, J.; Omori, M.; Whitten, J. P.; Anderes, K.; Rice, W. G.; Ryckman, D. M. Discovery of CX-6258. A potent, selective, and orally efficacious pan-Pim kinases inhibitor. *ACS Med. Chem. Lett.* **2012**, *3*, 135–139.
- (40) Blanco-Aparicio, C.; Collazo, A. M. G.; Oyarzabal, J.; Leal, J. F.; Albarán, M. I.; Lima, F. R.; Pequeño, B.; Ajenjo, N.; Becerra, M.; Alfonso, P.; Reymundo, M. I.; Palacios, I.; Mateos, G.; Quiñones, H.; Corriero, A.; Carnero, A.; Pevarello, P.; Lopez, A. R.; Forminaya, J.; Pastor, J.; Bischoff, J. R. Pim 1 kinase inhibitor ETP-45299 suppresses cellular proliferation and synergizes with PI3K inhibition. *Cancer Lett.* **2011**, *300*, 145–153.
- (41) Sliman, F.; Blairvacq, M.; Durieu, E.; Meijer, L.; Rodrigo, J.; Desmaële, D. Identification and structure–activity relationship of 8-hydroxy-quinoline-7-carboxylic acid derivatives as inhibitors of Pim-1 kinase. *Bioorg. Med. Chem. Lett.* **2010**, *20*, 2801–2805.
- (42) Olla, S.; Manetti, F.; Crespan, E.; Maga, G.; Angelucci, A.; Schenone, S.; Bologna, M.; Botta, M. Indolyl-pyrrolone as new scaffold for Pim1 inhibitors. *Bioorg. Med. Chem. Lett.* **2009**, *19*, 1512–1516.
- (43) Tsuganezawa, K.; Watanabe, H.; Parker, L.; Yuki, H.; Taruya, S.; Nakagawa, Y.; Kamei, D.; Mori, M.; Ogawa, N.; Tomabechi, Y.; Handa, N.; Honma, T.; Yokoyama, S.; Kojima, H.; Okabe, T.; Nagano, T.; Tanaka, A. A novel Pim-1 kinase inhibitor targeting residues that bind the substrate peptide. *J. Mol. Biol.* **2012**, *417*, 240–252.
- (44) Bain, J.; Plater, L.; Elliott, M.; Shpiro, N.; Hastie, C. J.; McLaughlan, H.; Klevernic, I.; Arthur, J. S. C.; Alessi, D. R.; Cohen, P. The selectivity of protein kinase inhibitors: a further update. *Biochem. J.* **2007**, *408*, 297–315.
- (45) cLogP values were calculated by ChemBioDraw Ultra, version 11.0.1 (CambridgeSoft).
- (46) Nassar, A.-E. F.; Kamel, A. M.; Clarimont, C. Improving the decision-making process in the structural modification of drug candidates: enhancing metabolic stability. *Drug Discovery Today* **2004**, *9*, 1020–1028.
- (47) Gleeson, M. P. Generation of a set of simple, interpretable ADMET rules of thumb. *J. Med. Chem.* **2008**, *51*, 817–834.
- (48) Oprea, T. I.; Davis, A. M.; Teague, S. J.; Leeson, P. D. Is there a difference between leads and drugs? A historical perspective. *J. Chem. Inf. Comput. Sci.* **2001**, *41*, 1308–1315.
- (49) PDB ID: 3UMX.
- (50) Friedmann, M.; Nissen, M. S.; Hoover, D. S.; Reeves, R.; Magnuson, N. S. Characterization of the proto-oncogene Pim-1: kinase activity and substrate recognition sequence. *Arch. Biochem. Biophys.* **1992**, *298*, 594–601.
- (51) Qian, K. C.; Wang, L.; Hickey, E. R.; Studts, J.; Barringer, K.; Peng, C.; Kronkaitis, A.; Li, J.; White, A.; Mische, S.; Farmer, B. Structural basis of constitutive activity and a unique nucleotide binding mode of human Pim-1 kinase. *J. Biol. Chem.* **2005**, *280*, 6130–6137.
- (52) Pierce, A. C.; Jacobs, M.; Stuver-Moody, C. Docking study yields four novel inhibitors of the protooncogene Pim-1 kinase. *J. Med. Chem.* **2008**, *51*, 1972–1975.
- (53) Cherry, M.; Williams, D. H. Recent kinase and kinase inhibitor X-ray structures: mechanism of inhibition and selectivity insights. *Curr. Med. Chem.* **2004**, *11*, 663–673.
- (54) Thaimattam, R.; Banerjee, R.; Miglani, R.; Iqbal, J. Protein kinase inhibitors: structural insights into selectivity. *Curr. Pharm. Des.* **2007**, *13*, 2751–2765.
- (55) Swahn, B.-M.; Huerta, F.; Kallin, E.; Malmström, J.; Weigelt, T.; Viklund, J.; Womack, P.; Xue, Y.; Öhberg, L. Design and synthesis of 6-anilinoindazoles as selective inhibitors of c-Jun N-terminal kinase-3. *Bioorg. Med. Chem. Lett.* **2005**, *15*, 5095–5099.
- (56) Perola, E. Minimizing false positives in kinase virtual screens. *Proteins* **2006**, *64*, 422–435.
- (57) Hopkins, A. L.; Groom, C. R.; Alex, A. Ligand efficiency: a useful metric for lead selection. *Drug Discovery Today* **2004**, *9*, 430–431.
- (58) Leeson, P. D.; Springthorpe, B. The influence of drug-like concepts on decision-making in medicinal chemistry. *Nature Rev. Drug Discovery* **2007**, *6*, 881–890.

(59) LE and LLE were calculated as follows: $LE = -1.4\log(IC_{50})$ / (number of heavy atoms), $LLE = -\log(IC_{50}) - cLogP$; Edwards, M. P.; Price, D. A. Role of physicochemical properties and ligand lipophilicity efficiency in addressing drug safety risks. *Annu. Rep. Med. Chem.* **2010**, *45*, 381–391.

(60) Tsai, J.; Lee, J. T.; Wang, W.; Zhang, J.; Cho, H.; Mamo, S.; Bremer, R.; Gillette, S.; Kong, J.; Haass, N. K.; Sproesser, K.; Li, L.; Smalley, K. S. M.; Fong, D.; Zhu, Y.-L.; Marimuthu, A.; Nguyen, H.; Lam, B.; Liu, J.; Cheung, L.; Rice, J.; Suzuki, Y.; Luu, C.; Settachatgul, C.; Shellooe, R.; Cantwell, J.; Kim, S.-H.; Schlessinger, J.; Zhang, K. Y. J.; West, B. L.; Powell, B.; Habets, G.; Zhang, C.; Ibrahim, P. N.; Hirth, P.; Artis, D. R.; Herlyn, M.; Bollag, G. Discovery of a selective inhibitor of oncogenic B-Raf kinase with potent antimelanoma activity. *Proc. Natl. Acad. Sci. U.S.A.* **2008**, *105*, 3041–3046.

(61) Kim, K.-T.; Levis, M.; Small, D. Constitutively activated FLT3 phosphorylates BAD partially through Pim-1. *Br. J. Haematol.* **2006**, *134*, 500–509.

(62) Kerns, E. H.; Di, L. *Drug-Like Properties: Concepts, Structure Design, and Methods*; Academic Press: New York, 2008.

(63) (a) Liu, X.; Gourley, E.; Lamb, J.; Grand, C.; Lloyd, M.; Warner, S.; Wolfe, B.; Bearss, D.; Vankayalapati, H. Discovery of SGI-1776, a potent and selective Pim-1 kinase inhibitor. AACR 2009 Annual Meeting, Denver, Colorado, April 18–22, 2009, Abstract No. 2013.

(b) While we were preparing the manuscript, Astex Pharmaceuticals reported that SGI-1776 inhibits hERG with IC_{50} value of 1 μ M. (http://astx.com/content/resources/2011_PIM_poster_EORTC_abstC200_Foulks.pdf): Foulks, J. M.; Xu, Y.; Saunders, M.; Liu, X.-H.; Brenning, B.; Clifford, A.; Wilkes, M.; Luo, B.; Lai, S.; Merx, S.; Chan, A.; Huang, L.; Vollmer, D.; Senina, A.; Liu, J.; Ho, K.; McCullar, M. V.; Kanner, S. B. Second-generation PIM inhibitors exhibit improved activity in solid tumor models in vitro. AACR-NCI-EORTC International Conference: Molecular Targets and Cancer Therapeutics, San Francisco, CA, Nov 12–16, 2011. *Mol. Cancer Ther.* **2011**, *10* (11, Suppl 1), Abstract no. C200.

(64) Chen, J.; Shi, Z.-F.; Zhou, L.; Xie, A.-L.; Cao, X.-P. Total synthesis of malyngamide M and isomalyngamide M. *Tetrahedron* **2010**, *66*, 3499–3507.

(65) (a) For the synthesis of 4-azaindole-3-aldehyde: Greenhouse, R.; Jamie-Figueroa, S.; Lynch, S. M.; Raptova, L.; Stein, K. A.; Weikert, R. J. 3-Amino-1-arylpropyl azaindoles and uses thereof. US 2007/0123535, 2007. (b) For the synthesis of 5-azaindole-3-aldehyde: Bradbury, R. H.; Hales, N. J.; Rabow, A. A. Bicyclic derivatives for use in the treatment of androgen receptor associated conditions. WO 2009/081197, 2009.

(66) Kigawa, T.; Yabuki, T.; Matsuda, N.; Matsuda, T.; Nakajima, R.; Tanaka, A.; Yokoyama, S. Preparation of *Escherichia coli* cell extract for highly productive cell-free protein expression. *J. Struct. Funct. Genomics* **2004**, *5*, 63–68.

(67) Matsuda, T.; Koshiba, S.; Tochio, N.; Seki, E.; Iwasaki, N.; Yabuki, T.; Inoue, M.; Yokoyama, S.; Kigawa, T. Improving cell-free protein synthesis for stable-isotope labeling. *J. Biomol. NMR* **2007**, *37*, 225–229.

(68) Kigawa, T.; Matsuda, T.; Yabuki, T.; Yokoyama, S. Bacterial cell-free system for highly efficient protein synthesis. In *Cell-Free Protein Synthesis: Methods and Protocols*; Spirin, A. S., Swartz, J. R., Eds.; Wiley-VCH: Weinheim, Germany, 2007; pp 83–97.

(69) Jacobs, M. D.; Black, J.; Futer, O.; Swenson, L.; Hare, B.; Fleming, M.; Saxena, K. Pim-1 ligand-bound structures reveal the mechanism of serine/threonine kinase inhibition by LY294002. *J. Biol. Chem.* **2005**, *280*, 13728–13734.

(70) Leslie, A. G. W. Recent changes to the MOSFLM package for processing film and image plate data. *Joint CCP4 + ESF-EAMCB Newsletter on Protein Crystallography* **1992**, *26*.

(71) Collaborative Computational Project, Number 4. The CCP4 suite: programs for protein crystallography. *Acta Crystallogr., Sect. D: Biol. Crystallogr.* **1994**, *50*, 760–763.

(72) McCoy, A. J.; Grosse-Kunstleve, R. W.; Adams, P. D.; Winn, M. D.; Storoni, L. C.; Read, R. J. *Phaser* crystallographic software. *J. Appl. Crystallogr.* **2007**, *40*, 658–674.

(73) Murshudov, G. N.; Vagin, A. A.; Dodson, E. J. Refinement of macromolecular structures by the maximum-likelihood method. *Acta Crystallogr., Sect. D: Biol. Crystallogr.* **1997**, *53*, 240–255.

(74) Emsley, P.; Cowtan, K. *Coot*: model-building tools for molecular graphics. *Acta Crystallogr., Sect. D: Biol. Crystallogr.* **2004**, *60*, 2126–2132.